ACS NANO
Cite This: ACS Nano 2018, 12, 2292–2310
www.acsnano.org

ARTICLE

Short-Term Pulmonary Toxicity Assessment of Pre- and Post-incinerated Organomodified Nanoclay in Mice

Todd A. Stueckle,*[,†] Donna C. Davidson,[†] Ray Derk,[†] Tiffany G. Kornberg,[†,‡] Lori Battelli,[†] Sherri Friend,[†] Marlene Orandle,[†] Alixandra Wagner,[§] Cerasela Zoica Dinu,[§] Konstantinos A. Sierros,[∥] Sushant Agarwal,[§] Rakesh K. Gupta,[§] Yon Rojanasakul,[‡] Dale W. Porter,[†] and Liying Rojanasakul[†]

[†]Health Effects Laboratory Division, National Institute for Occupational Safety and Health, Morgantown, West Virginia 26505, United States

[‡]Department of Basic Pharmaceutical Sciences, [§]Department of Chemical and Biomedical Engineering, and [∥]Department of Mechanical and Aerospace Engineering, West Virginia University, Morgantown, West Virginia 26506, United States

Supporting Information

ABSTRACT: Organomodified nanoclays (ONCs) are increasingly used as filler materials to improve nanocomposite strength, wettability, flammability, and durability. However, pulmonary risks associated with exposure along their chemical lifecycle are unknown. This study's objective was to compare pre- and post-incinerated forms of uncoated and organomodified nanoclays for potential pulmonary inflammation, toxicity, and systemic blood response. Mice were exposed *via* aspiration to low (30 μg) and high (300 μg) doses of preincinerated uncoated montmorillonite nanoclay (CloisNa), ONC (Clois30B), their respective incinerated forms (I-CloisNa and I-Clois30B), and crystalline silica (CS). Lung and blood tissues were collected at days 1, 7, and 28 to compare toxicity and inflammation indices. Well-dispersed CloisNa caused a robust inflammatory response characterized by neutrophils, macrophages, and particle-laden granulomas. Alternatively, Clois30B, I-Clois30B, and CS high-dose exposures elicited a low grade, persistent inflammatory response. High-dose Clois30B exposure exhibited moderate increases in lung damage markers and a delayed macrophage recruitment cytokine signature peaking at day 7 followed by a fibrotic tissue signature at day 28, similar to CloisNa. I-CloisNa exhibited acute, transient inflammation with quick recovery. Conversely, high-dose I-Clois30B caused a weak initial inflammatory signal but showed comparable pro-inflammatory signaling to CS at day 28. The data demonstrate that ONC pulmonary toxicity and inflammatory potential relies on coating presence and incineration status in that coated and incinerated nanoclay exhibited less inflammation and granuloma formation than pristine montmorillonite. High doses of both pre- and post-incinerated ONC, with different surface morphologies, may harbor potential pulmonary health hazards over long-term occupational exposures.

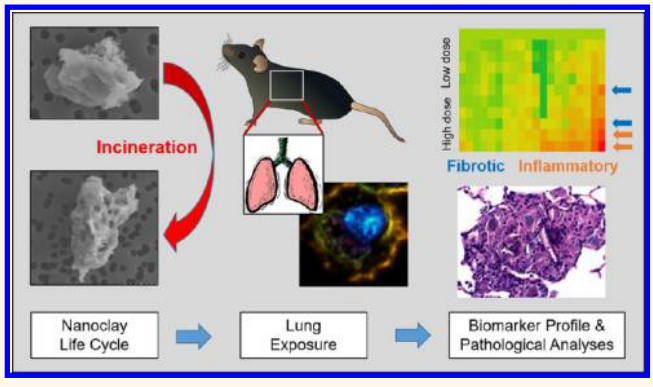

KEYWORDS: *inflammation, life cycle, nanoparticles, pulmonary, toxicity*

Organomodified nanoclays (ONCs), natural clays coated with organic modifiers, represent an engineered nanomaterial (ENM) class that possesses the ability to achieve high dispersibility in composite material.[1,2] ONC-enabled composites, with marked improvement in numerous physicochemical characteristics, have allowed for their wide use and application across commercial, industrial, and construction sectors.[3,4] With such a large expansion of the ONC-enabled composite market, occupational airborne ONC exposures are forecasted to increase;[5] however, extremely little is known about inhalation and resulting pulmonary toxicity.[6]

Specifically, montmorillonite represents a major class of nanoclay with favorable physicochemical characteristics for organic modifier coatings to assist in adequate dispersion in plastic composite materials.[1,7] Montmorillonite is a 2:1 phyllosilicate smectite deposit with platelet-shaped morphology composed of two SiO_2 tetrahedral sheets bounding an alumina

Received: October 13, 2017
Accepted: February 16, 2018
Published: February 16, 2018

DOI: 10.1021/acsnano.7b07281
ACS Nano 2018, 12, 2292–2310

octahedral sheet. Mg^{2+}, Fe^{2+}, and Al^{3+} substitutions within the sheets produce a negative charge that is counterbalanced with occasional Na^{+} and Ca^{2+} deposits within the interlayers. The resulting single platelets are typically 1 nm thick and 200−500 nm in length and width dimensions, thus classifying them as high aspect ratio (HAR) particles. Given the ionic surface charge in the galleries between each particle, platelets are usually stacked resulting in agglomerate particles in the fine particle scale;[1,7,8] however, manipulation of these materials results in particle size distributions well within the nano- and fine particle fractions.[9,10] Exposure to airborne montmorillonite results in robust pulmonary inflammation, persistent lung particle burdens, silicosis-like lesions, and pneumoconiosis in humans and *in vivo* models.[2,11−14] Although past nanoclay composite materials have used montmorillonite as filler material, their application is less than desirable since hydrophilic nanoclay does not disperse well in plastic polymers, thus providing only moderate strength characteristics. Recent advances in polymer chemistry have resulted in addition of coatings comprised of quaternary ammonium compounds (QACs) with short or long alkyl chains that enter the intergallery spaces between nanoclay platelets. Through an ion-exchange process, a hydrophobic and functional surface results, which provides excellent platelet exfoliation and dispersion in plastic base composites.[15,16] Well-dispersed ONC-enabled composites demonstrate water and gas impermeability, excellent flame retardant characteristics, reduced aqueous surface tension/friction, improved strength and flexibility, and durability. Given their low cost, widespread availability, and compatibility with petroleum and "green" plant-based polymers, ONC-enabled composites are projected to experience wide use across the plastic industry including thin films, electronics, coatings, flame retardant surfaces, durables, wovens, fabric, and 3D printing applications.[17−19] Consumer and industrial uses include automobile and aerospace parts, food wrapping, plastic wrap, pipe coatings, low flammable coatings, and durable consumer goods/cases.[3,20,21]

Recent research to assess ONC exposure health impacts has begun to use a life cycle approach, which includes production, transport, use, breakdown, and disposal considerations.[17,18] A life cycle modeling study of ONC polypropylene composite found several instances for potential occupational exposure during ONC synthesis, milling, bagging, composite synthesis with molding or extrusion, and waste incineration.[22] Two human occupational exposure studies reported airborne ONC concentrations ranging from 5.2 to 39.2 mg/m^3 and 7.73 to 12.73 mg/m^3 following ONC synthesis, which included pulverization and packaging activities with no dust removal control strategies.[23,24] Limited particle exposure studies report the release of nano- and submicron particles during both ONC composite synthesis and breakdown.[10,25,26] Recent reviews of ENM exposure studies highlighted ONCs as an ENM class for potential occupational exposure, but with little exposure or toxicological effect data to assess occupational risks.[5,27] Airborne ultrafine particulate studies identified nanosized particulate containing Ca and Al as a significant portion of fly ash following waste incineration.[28] Incineration is projected as a major end-of-life stream for nanomaterials, which poses several challenges in understanding how to potentially control particle transformation, filtering, and fate.[18,29] Moreover, nanomaterial filler may influence the behavior of plastic composite and affect fly ash structure and chemical composition during incineration.[30]

Currently, a majority of ONC toxicity data has been conducted in gastrointestinal *in vivo* and *in vitro* models given the interest in ONC composite thin film applications for food wrappings. *In vitro* studies indicate that ONCs caused increased oxidative stress, changes in Golgi apparatus structure, genotoxicity, and mitochondrial degeneration with indication that the organic modifier was driving the toxicological effect.[6,31−33] However, *in vivo* gastrointestinal exposure studies showed little to no inflammation, ROS, genotoxicity, nor tissue damage in the intestine, liver, and kidney. Very few data exist evaluating inflammatory responses to ONCs compared to the robust pristine montmorillonite literature. Similarly, little is known about inhalation ONC exposure and the resulting pulmonary toxicity and immunomodulatory effects.[6]

Given the projected increase in airborne occupational exposure and the lack of pulmonary toxicity data of ONCs across their life cycle, this study's main objective was to assess and characterize pulmonary inflammation and airway damage following exposure to pre- and post-incinerated uncoated and organomodified nanoclay. We hypothesized that the presence of the organic coating would cause lower inflammation but higher cytotoxicity than pristine uncoated nanoclay upon pulmonary exposure and, upon incineration, produce differential responses in exposed pulmonary tissue. C57Bl/6J mice were exposed to either 30 or 300 μg per mouse *via* a single oropharyngeal aspiration to pre- or post-incinerated pristine uncoated or organomodified montmorillonite. Doses were based on deposited montmorillonite and crystalline silica (CS) doses used in previous chronic rat inhalation studies that model human occupationally relevant exposures.[34,35] Heat inactivated CS exposure served as a benchmark control particle based on similar chemical composition, size, and a robust pulmonary toxicity literature. Furthermore, use of CS provides an opportunity to compare toxicity mechanisms of nanoclay. Lung damage and inflammation end points were assessed in collected bronchoalveolar lavage fluid (BALF), lung tissue sections, and lung homogenates at 1, 7, and 28 days postexposure. In addition, systemic circulatory effects were measured by monitoring blood cell differentials and platelet activation. This study provides data linking changes to physicochemical properties of an ONC material across its prospective life cycle to pulmonary inflammation response and adverse effects. By conducting this evaluation in a comparative particle and dose−response framework, the effect of presence/absence of organic polymer coating and pre/post-incineration that primarily influence inflammation response can improve prevention by design strategies to safe guard against adverse outcomes following occupational exposure.

RESULTS AND DISCUSSION

Limited exposure studies along the forecasted ONC lifecycle indicate the potential for airborne respirable particle release with maximum levels reported at 12.73 and 39.2 mg/m^3 during ONC synthesis[24] and 131000 particles/cm^3 released from ONC composite materials.[10] However, no study has investigated *in vivo* pulmonary exposure to ONCs or their incinerated end-of-life byproducts. This study evaluated pulmonary risks associated with pre- and post-incinerated ONC *in vivo* exposure. Mice were aspirated to 30 μg or 300 μg of pre- or post-incinerated uncoated (CloisNa) or coated ONC (Clois30B) and evaluated for changes in BALF cellularity, BALF cytokine profile expression, and lung histopathology at 1, 7, and 28 days postexposure. This study provides information

DOI: 10.1021/acsnano.7b07281
ACS Nano 2018, 12, 2292−2310

Table 1. Pre- and Post-incinerated Organomodified Nanoclay Physicochemical Properties[a]

parameter	particle				
	Clois Na	Clois 30B	I-Clois Na	I-Clois 30B	CS
supplier	Southern Clay Products	Southern Clay Products	WVU Engineering	WVU Engineering	Min-U-Sil 5, US Silica
coating	uncoated	methyl, tallow, bis-2-hydroxyethyl, quaternary ammonium	900 °C incineration	900 °C incineration	uncoated, heat inactivated
ρ (g/cm^3)	2.86	1.98	ND	ND	2.65
BET surface area (m^2/g)	800[b]	7.74[c]	ND	ND	5.1[d]
d_h saline (nm)	380.7 ± 10.4	1941.1 ± 183.7	1537 ± 305.7	3228 ± 533	1023 ± 288.6
PDI	0.262	0.841	0.817	0.804	0.645
peak 1 (nm)	438.8 (96.5%)	409.3 (100%)	493.5 (100%)	805.5 (100%)	690.4 (100%)
peak 2 (nm)	113.8 (3.4%)	ND	ND	ND	ND
ζ saline (mV)	−43.8	−25.4	−35.9	−25.9	−27.9
EDX platelet	Al, Si, C, O, (K)	Al, Si, C, O, (P, Fe, Cl)	Al, Si, C, O, (Fe)	Al, Si, C, O, (Fe)	Si, O
EDX colloid	Al, Si, O, (K)	Al, Si, C, O, (P, Fe)	Al, Si, O	Al, Si, O	n/a

[a]ρ = density; d_h = hydrodynamic diameter; ζ = zeta potential; ND = not determined. [b]Reference 39. [c]Reference 40. [d]Reference 41. [e]Loose agglomerates of colloidal aluminum silicate were present.

on how physicochemical properties associated with QAC coating and incineration status impact lung inflammation and toxicity and potentially identify differences in underlying mechanism.

Particle Characterization of Dispersed Pre- and Post-incinerated ONCs. Given recent evidence for airborne ONC occupational exposures with unknown pulmonary health risks, this study builds upon recent ONC life cycle particle characterization and *in vitro* toxicity reports[36,37] by assessing dispersed particle physicochemical properties and how they potentially influence *in vivo* particle deposition and pulmonary inflammation and toxicity response. Initial particle characterization results were reported in Wagner *et al.*[36] Briefly, FTIR analysis of both preincinerated nanoclays confirmed the presence of the QAC modifier on Clois30B, while both nanoclays exhibited Si−O−Si (1000 cm^{-1}) and Al−OH−Al (900 cm^{-1}) peaks. Following incineration, however, all peaks associated with organic material had disappeared, which was confirmed by TGA analyses and SEM/EDX, demonstrating a 35% mass loss and little surface carbon present, respectively. Shifts in both Si−O−Si and Al−OH peaks occurred for both incinerated nanoclays, suggesting deformation of these bonds and dehydroxylation of nanoclay structure known to occur at 700 °C, resulting in formation of amorphous surface morphologies. Notably, I-CloisNa retained a more pronounced Si−O−Si (640 cm^{-1}) than I-Clois30B, indicating that I-CloisNa may possess surface activity associated with pyrogenic silica.[38]

Hydrodynamic light-scattering analysis (DLS) of all dispersed particles in saline suspension indicated that CloisNa exhibited well-dispersed bimodal size distribution (d_h = 380.7) with 97% of particles at a mean peak of 438.8 nm, while 3% exhibited sizes approaching nanosized range (113.8 nm; Table 1). Conversely, Clois30B with its hydrophobic coating exhibited polydisperse suspension (d_h = 1941 nm), including a 409.3 nm peak. Overagitation (*e.g.*, excessive handling) of sonicated Clois30B suspension caused mild reagglomeration of submicron-dispersed particles due to their hydrophobic nature resulting in a peak shift from 141 to 675.3 nm over a 6 min time span. Both incinerated nanoclays exhibited polydisperse suspensions similar to Clois30B, but did not show hydrophobic reagglomeration. I-CloisNa (d_h = 1537) exhibited near 50% smaller particle sizes than I-Clois30B, with a submicron peak at 493.5 nm. Conversely, I-Clois30B exhibited a d_h = 3228 with a peak at 805 nm. CS exhibited uniform and stable dispersion at d_h = 1023 nm. On the basis of the fast settling rate of agglomerates in polydisperse samples, peaks for large single micron particles were not reliably determined by the Zetasizer software.

FESEM/EDX analysis largely supported the DLS data. Both CloisNa and Clois30B exhibited both single and stacked platelet morphologies with CloisNa harboring more well-dispersed single platelets (Figure 1a and b). EDX surface chemical analysis identified Al, Si, C, and O on both particles with occasional focal detection of K, Fe, and P (Table 1; Supplemental Figure 1). Conversely, both I-CloisNa and I-Clois30B possessed amorphous structure typical of pyrogenic silica.[38,42] However, a substantial fraction of I-Clois30B exhibited a porous particle structure with some evidence of residual platelike structure, possibly due to interactions of the organic modifier and deformation of Si−O or Al−O bonds during incineration.[43] It is possible that (a) an interaction between the organic compounds that come off in stages due to interactions with Si−O or Al−O bonds and (b) increased spacing between platelets due to presence of the organic modifier resulted in creation of pores within the stacked platelet structure.[43] Incineration clearly caused larger agglomerates to form for both nanoclays due to deformation of Si−O bonds,[36] with I-Clois30B possessing close to a unimodal dispersion around 1 μm while I-CloisNa exhibited bimodal distribution. Fe deposits were evident on both preincinerated CloisNa and both post-incinerated nanoclays characterized by bright raised areas on particle surface, and were confirmed by EDX analysis. Of note, a small fraction of all four nanoclay samples was composed of colloidal Al/SiO_2 agglomerates (Figure 1b,e). No evidence of colloidal aluminum silicate was found in water used to make stock solutions and CS samples.

Since platelet-shaped particles exhibit aerodynamics that influence pulmonary deposition, estimation of particle aerodynamic diameter (D_{ae}) for nanoclays with underlying platelet morphology was determined. D_{ae} calculations indicated that the 438 nm fraction of CloisNa was less than 698 nm in size (Supplemental Figure 2). Given the well-dispersed nature of CloisNa with minimal detection of agglomerates approaching 1 μm thickness, a majority of CloisNa was estimated to be below 310 nm. The submicron fraction of Clois30B showed

DOI: 10.1021/acsnano.7b07281
ACS Nano 2018, 12, 2292−2310

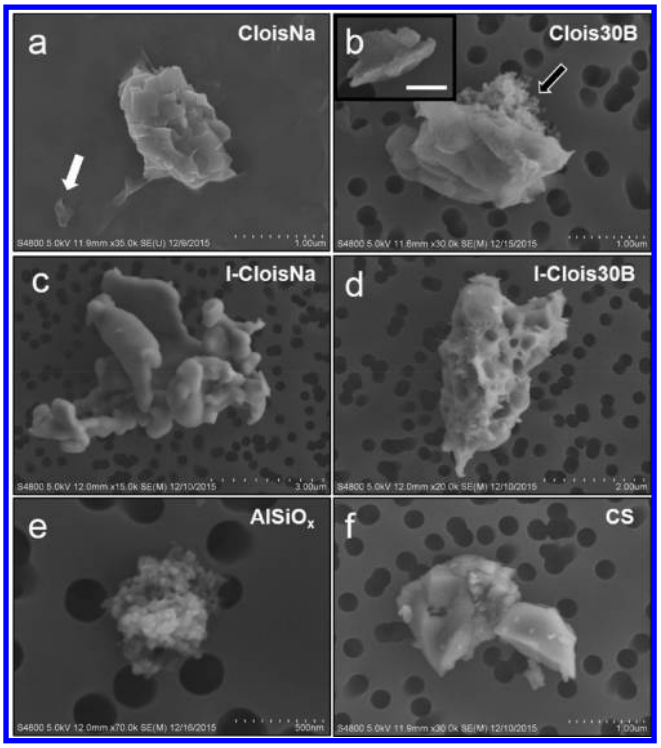

Figure 1. FESEM characterization of dispersed pre- and post-incinerated nanoclays in saline vehicle. (a) Single (white arrow) and stacked platelets of pristine CloisNa and (b) organomodified Clois30B exhibited stacked or exfoliated platelet morphology with occasional detection of colloidal aluminum silicate agglomerates (black arrow). Inset shows exfoliated platelet with 250 nm scale bar. (c) I-CloisNa possessed a large, amorphous particle structure, while (d) I-Clois30B exhibited either a smooth or pocketed structure. (e) Aluminum silicate colloids were observed in all samples. (f) Heat-inactivated crystalline silica.

comparable D_{ae} (789 and 250 nm) to CloisNa. However, the d_h of Clois30B exhibited D_{ae} at 2430 nm, indicating that large agglomerates were close to the upper limit (~3 μm) of a respirable particle. These D_{ae} data suggested that both preincinerated nanoclay particles were within respirable fraction range for the mouse and human lung.[44,45] Based on nonplatelet morphology of incinerated nanoclays and CS, D_{ae} was not calculated. These dispersed particle size distributions closely matched those expected during machining or breakdown in occupational settings and indicated that the resulting size fractions were respirable in the mouse *in vivo* pulmonary exposure model. Pristine montmorillonite is well-known to possess dustiness qualities with airborne single micron particle sizes, while ultrafine particle size ranges are generated following mechanical manipulation of natural deposits including mining, processing, and ball milling.[46] On the basis of CloisNa's silica and aluminum oxide chemistry,[36] negative surface charge, and negative zeta potential in solution, this uncoated nanoclay was easily dispersed in saline with a majority within the size range expected for either single platelet or small stacked platelet aggregates, which closely matched those reported in occupational exposures. Comparatively, dispersion of Clois30B in aqueous solutions indicated that the QAC tallow coating possessed hydrophobic tendencies, which resulted in larger particle size distribution for the smaller particle fraction. Several studies of nanoalumina and ONC simulated exposures reported size ranges during manufacturing (30–75 nm), nanoclay composite synthesis (50–600 nm), and composite breakdown (255–459 nm) that match our suspended size distributions.[9,10,25] Conversely, dustiness or mild sonication suspensions resulted in submicron to large single micron particles in both pristine nanoclays and ONCs.[26,36,47] Next, minimal endotoxin was detected in all particle suspensions (≤0.07 EU/mL) with no significant difference observed among particles or with blank controls (Table 2). Both preincinerated nanoclays were observed to bind significantly more internally spiked lipopolysaccharide (LPS) than post-incinerated nanoclays and CS ($p < 0.05$).

Table 2. Endotoxin Levels in UV or Heat-Inactivated Samples

particle	endotoxin (Eu/ml)	LPS bound in internal spike (%)
CloisNa	0.07 ± 0.08	63.5[a]
Clois30B	0.05 ± 0.08	53.1[a]
I-CloisNa	0.06 ± 0.08	28.7[a]
I-Clois30B	0.06 ± 0.08	45.4[a]
crystalline silica (heat inactivated)	0.07 ± 0.08	6.4

[a]Significant differences compared to benchmark particle ($p < 0.05$).

Nanoclay Deposition in the Deep Lung Coincided with Its Aerodynamic Diameter. Particles with platelet or stacked platelet morphologies can exhibit physicochemical properties that dictate their aerodynamic behavior and respirable potential that determines deep lung deposition.[48,49] A platelet's or platelet agglomerate's movement is a function of its lateral size, layer number, aerodynamic resistance force, and density. Based on calculations with graphene platelets,[48,49] substantial deposition in the respiratory tract can occur across a wide range of lateral dimensions, with submicron layered platelet particles reaching near 50% deposition in the alveolar region. Evaluation of H & E stained lung sections of day 1 300 μg-dosed animals indicated that CloisNa deposited primarily in the terminal bronchioles (TB), alveolar ducts (AD), and alveoli (Figure 2a), confirming D_{ae} estimates of deep lung deposition. Particles appeared as abundant fine, grainy, bluish material, which often coated alveolar walls and filled airspaces. Polarizing light microscopy revealed that CloisNa was poorly birefringent, possibly due to abundant and overlapping nature of these platelet-shaped particles (Figure 2b). Given the submicron lateral dimensions, single nanometer thickness, and well-dispersed nature of hydrophilic CloisNa, polarized light and enhanced dark field imaging were not preferable methodologies to visualize pristine nanoclay in exposed lung tissue. Compression of single or several layers of nanoclay within lung sections could effectively block a majority of scattered or polarized light.[48] FESEM/EDX analysis of serial lung sections indicated that blue, grainy deposits at both AD and in alveolar airspaces contained Si, Al, Na, and occasional Fe and Mg, thus confirming CloisNa deposition (Figure 2b, upper right). Conversely, Clois30B exhibited variably sized particles with large agglomerates primarily depositing in the TB and AD, whereas single platelet and small agglomerate deposits were seen within the alveoli. These deposition data with single and stacked platelets correlated well with the Clois30B D_{ae} estimate. These data were consistent with modeled D_{ae} and known deposition patterns of single micron and submicron platelet-shaped particles in the deep lung.[48,49] Both I-CloisNa and I-

DOI: 10.1021/acsnano.7b07281
ACS Nano 2018, 12, 2292–2310

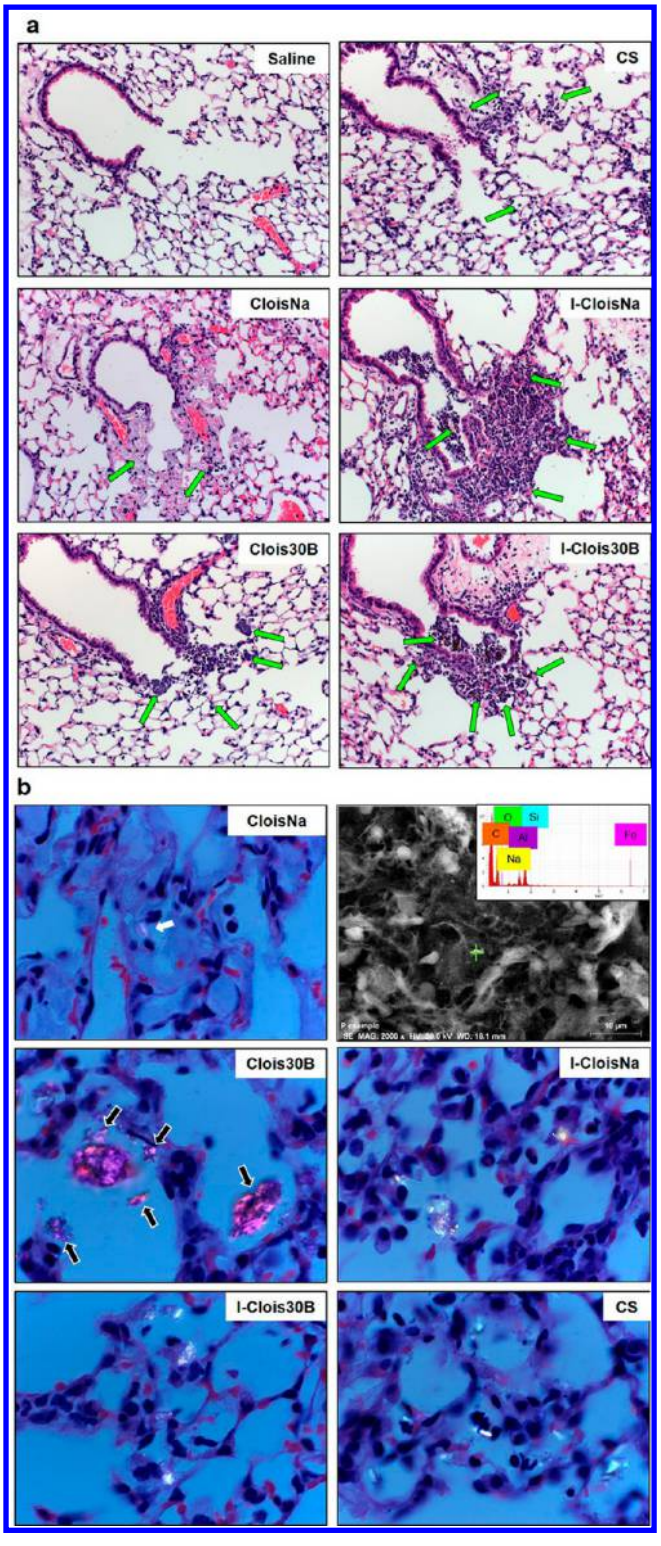

Figure 2. Deposition of pre- and post-incinerated organomodified montmorillonite nanoclay (300 μg/mouse) in day 1 postexposure animals. (a) H & E staining of terminal bronchiole (TB) and alveolar duct (AD) of exposed lung. 100× magnification. Green arrows indicate deposited particle associated with alveolar macrophages. (b) Polarized light microscopy of deposited particle in AD and alveoli of exposed lung. Images show particles (white) with polarized filter. 1000× magnification. CloisNa deposited in TB and AD regions as loose, stacked agglomerates or loosely dispersed in alveoli as small clusters and showed low polarization imaging potential (white arrows). FESEM/EDX elemental analysis confirmation of CloisNa within alveolar space (b, upper right). Clois30B was primarily found in TB and AD as large aggregates, with small aggregates in alveoli regions (black arrows). Both I-CloisNa and I-Clois30B deposited primarily in TB and AD regions, while crystalline silica was found well-dispersed in alveoli.

Figure 2. continued

Clois30B primarily deposited in TB and AD with minimal alveolar deposition. CS exhibited well-disbursed particle and deep alveolar deposition. All particle deposition in day 1 animals was confirmed with enhanced darkfield imaging (Supplemental Figure 3).

QAC Coating Reduced Acute Leukocyte Recruitment Associated with Uncoated Nanoclay but Caused Low, Persistent Elevated Macrophage Counts in Exposed Lung. All tested particle exposures produced significant particle-, dose-, and time-dependent increases in cell numbers in collected BALF. All high-dose particle exposures resulted in significantly elevated BALF cell numbers on day 1 with decreasing counts over time (Figure 3A), except for Clois30B and CS. CloisNa-exposed mice exhibited a robust, dose-

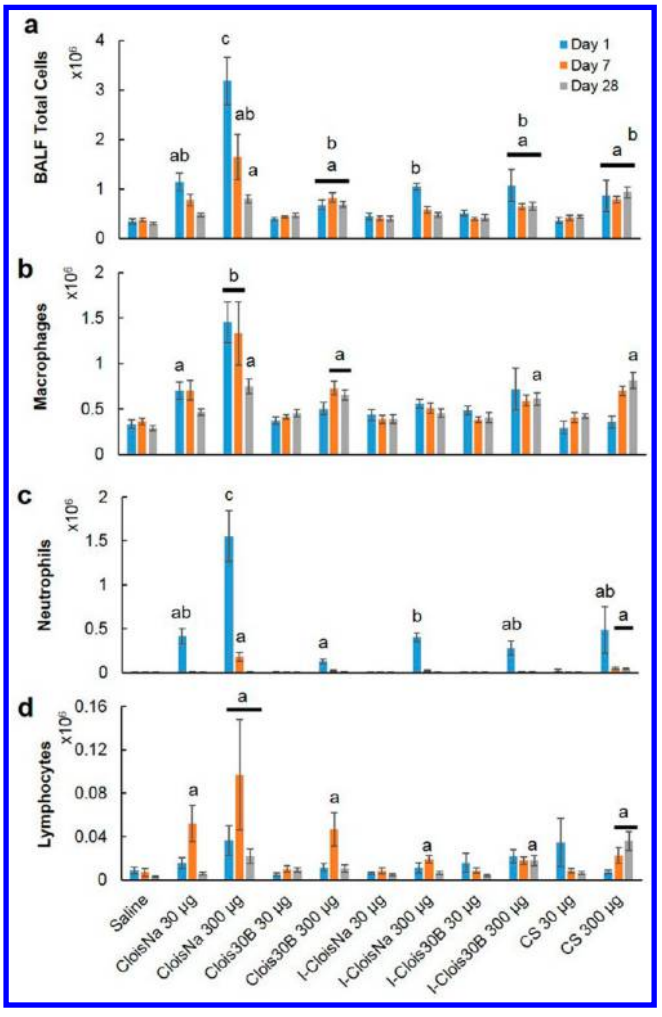

Figure 3. Bronchoalveolar lavage cell differential analysis following pre- and post-incinerated organomodified nanoclay exposure. (a) Total cell counts, (b) macrophages, (c) neutrophils, and (d) eosinophils. Different letters indicate those treatments significantly different from each other ($p < 0.05$, $n = 8$).

DOI: 10.1021/acsnano.7b07281
ACS Nano 2018, 12, 2292–2310

dependent 9-fold increase in cell counts which reduced over time (4.8- and 2.4-fold, respectively). Conversely, high-dose Clois30B-, I-Clois30B-, and CS-exposed mice experienced moderate significantly elevated infiltrates (2.0 to 3.1-fold) on day 1 that persisted to day 28. Clois30B cell counts peaked at day 7, while CS cell counts peaked at day 28. Only low-dose CloisNa and high-dose I-CloisNa exposure caused a significantly elevated cell count on day 1 that resolved by day 7. BALF samples from both low- and high-dose CloisNa at day 1 possessed an enhanced number of erythrocytes. Both low- and high-dose CloisNa-exposed animals experienced a significant increase (2- and 4.3-fold, respectively) in macrophages at day 1 postexposure compared to controls, while all other treatments showed no change (Figure 3b). These levels remained elevated through day 7 and dropped to near control levels by day 28. Large numbers of BALF macrophage and erythrocytes was consistent with known pulmonary damage following montmorillonite exposure.[38,45,50] BALF cytospin analysis revealed macrophages laden with CloisNa and Clois30B at each time point (Supplemental Figure 4a). Conversely, high-dose Clois30B animals experienced a significant 2-fold increase in macrophage infiltrate at day 7 and day 28. High-dose I-Clois30B and CS elicited significantly elevated macrophage counts (2.1- and 2.8-fold) at day 28.

Mean percentage of neutrophils and eosinophils in BALF ranged from 18 to 48.8% and 3.5 to 7.2%, respectively, of airway infiltrate response for high-dose particles on day 1 (Figure 3c and Supplemental Figure 4b). Specifically, high-dose CloisNa resulted in BALF with 48% neutrophils at day 1, which remained significantly elevated (10%) at day 7. Only CS exposure exhibited a persistent, elevated neutrophil presence in the airways (4.6%) to day 28. Both Clois 30B and I-Clois 30B displayed elevated neutrophil airway infiltrate responses (2 to 3%); however, these were the weakest responses compared with the other particles. All high-dose particle exposures caused significantly elevated eosinophil counts (1 to 5%) at days 1 and 7, which resolved by day 28. High-dose Clois 30B, I-Clois 30B, and CS showed the weakest eosinophil response (1 to 2%) at day 1. Low-dose particle exposure did not induce changes in eosinophilic counts relative to control.

Lymphocyte counts were significantly elevated (1 to 5%) at day 7 postexposure for low- and high-dose CloisNa, high-dose Clois30B, and high-dose I-CloisNa (Figure 3d). Lymphocyte counts increased over time for high-dose CS-exposed animals, while high-dose I-Clois30B animals showed elevated counts at day 28. These findings, along with elevated macrophage counts, suggested that incinerated ONC potentially harbors chronic pro-inflammatory properties similar to CS.[13,51−53] Interestingly, high-dose Clois30B at day 7 and day 28 and high-dose CS at day 28 caused a significant elevation in BALF binucleated macrophages (Supplemental Figure 4c), which represented 20% and 13% of the total BALF macrophage population, respectively.

QAC Coating Delayed Airway Damage and Cytotoxicity of Preincinerated Uncoated Nanoclay. Lung cytotoxicity and airway−blood barrier damage (by BALF LDH and total protein levels, respectively) was particle-, dose-, and time-dependent (Figure 4; $p < 0.0001$). Specifically, both high-dose pre- and post-incinerated CloisNa nanoclay elicited significant 6- and 3-fold increases, respectively, in BAL cytotoxicity (LDH) levels at day 1, which reduced over time. Dispersed montmorillonite represents an aluminosilicate HAR particle with silanol and aluminum oxide surface groups that are

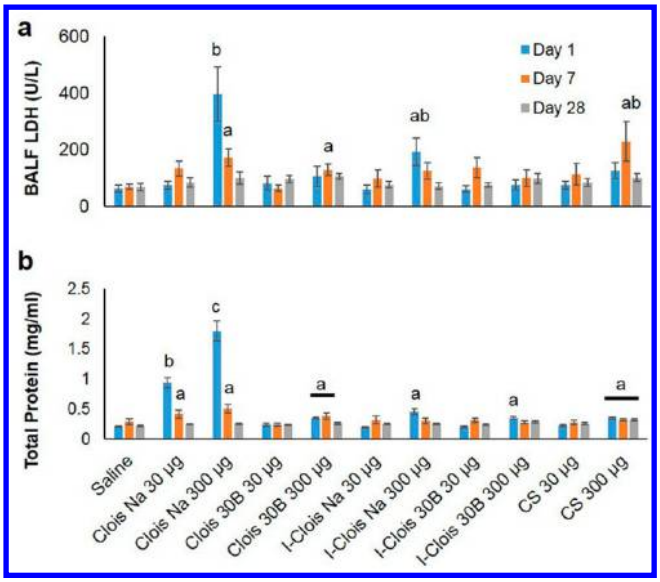

Figure 4. Cytotoxicity (LDH activity; a) and airway damage (total protein; b) markers in collected BAL fluid following pre- and post-incinerated organomodified nanoclay pulmonary exposure. Different letters indicate those treatments significantly different from each other ($p < 0.05$, $n = 8$).

well known to cause biological membrane damage and a robust inflammatory response.[38,54] Moreover, two recent studies report that pristine montmorillonite or nanoalumina particles may aggressively bind lung surfactant resulting in disruption of the biofluidic properties of the lung lining fluid,[55,56] potentially resulting in loss of the protective coating over epithelial cells and interfere with proper gas exchange.

Although not elevated on day 1, both high-dose Clois30B and CS exposure caused significant 2- and 3.3-fold increases, respectively, in cytotoxicity on day 7 only. Both low- and high-dose CloisNa elicited robust significant 4.6- and 8.6-fold increases in BALF LDH and total protein, respectively, which subsided back to control levels by day 28. Both Clois30B and CS caused a mild significant 1.7-fold increase in BALF LDH, which persisted to day 7 and day 28, respectively. These findings of no acute Clois30B-induced airway cellular damage and minimal macrophage or neutrophil infiltrate is in contrast with results typically reported in *in vitro* studies.[6] The organic coating may have shielded against surface silanol groups, aluminum oxide, and other bound ions (*e.g.*, Ca, Fe) with known abilities to induce cytotoxicity,[38] from coming in direct contact with macrophage and epithelial cells in the TB and alveoli. In addition, lung surfactant binding, less surface area per delivered mass compared to CloisNa, and dissolution rate of the QAC coating may have delayed and partially inhibited an acute cytotoxic response.

Traditional uses of QAC compounds include antimicrobial and preservative applications including nasal sprays, eye drops, and workplace disinfectants. Acute exposure to a potent QAC (benzalkonium chloride) alone is reported to cause epithelial cell and neutrophil apoptosis and cytotoxicity *via* membrane lysis.[57−59] Previous *in vitro* studies with Clois30B and other ONCs with different QAC modifiers reported cytotoxicity, ROS, altered mitochondrial and golgi apparatus structure, DNA damage, and apoptosis,[33,60−62] while ONCs with other organic coatings report no toxicity, even at extremely high doses.[6] Of note, Janer *et al.*[31] reported that the organic modifier drove

DOI: 10.1021/acsnano.7b07281
ACS Nano 2018, 12, 2292−2310

observed adverse responses across five different cell lines. Our previously published study reported that Clois30B exhibited significant bronchial epithelial cytotoxicity compared to CloisNa.[36] In this study, the delayed cytotoxic and total cell infiltrate response to Clois30B, comprised of macrophages and lymphocytes, compares to other submicron and ultrafine particles known to exhibit a delayed inflammatory response. Particles containing partly soluble metal species, such as welding fume particulate, quantum dots, and ZnO nanoparticles, can exhibit a weak acute inflammatory response followed by a delayed robust inflammation and pulmonary cytotoxicity, in part due to slow dissolution of metal ions from the deposited particle.[63−65] This suggests the possibility that the QAC coating on an ONC may undergo slow dissolution once deposited in the deep lung.

Postincinerated nanoclays (I-CloisNa and I-Clois30B) showed mild significant increases in cytotoxicity and barrier damage at only day 1, which is typical of large single micron silica particle exposures.[38] Animals exposed to CloisNa experienced a significant 13% decrease in body weight when compared to vehicle-only animals, which resolved at day 7 for low-dose-exposed animals (Supplemental Figure 5). High-dose-exposed animals gained weight by day 28, however, weight gain was significantly below (24%) control animals. The decreased body weight in CloisNa-exposed animals at day 1 may partially be explained by reduced oxygen availability,[55,56] reduced basal aerobic respiration, increased acute stress, reduced food intake, and use of systemic glycogen stores *via* anaerobic respiration.

QAC Coating and Incineration Status Influenced Time-Dependent Lung Inflammatory and Fibrotic Cytokine Signatures. A majority of the 20 assayed BALF cytokine expression was particle-, dose-, and time-dependent ($p < 0.0001$). IL-1β and FGFβ levels at day 1 were significantly elevated ($p < 0.032$) for every exposure group compared to controls and day 7 and day 28 animals. On day 1 postexposure, all high-dose particle- and low-dose CloisNa-exposed animals exhibited significant increase in pro-inflammatory (*e.g.* IL-6), macrophage (*e.g.*, MIP-1α and MIP-2), PMN chemokines (e.g., GM-CSF), and tissue damage markers (*e.g.*, Il-6 and TNFα) (Figure 5, Supplemental Table 1). Of these, both doses of CloisNa and high-dose I-CloisNa elicited the strongest response with 16 and 15 significantly elevated cytokines ranging 1.7-to 2060-fold, respectively, above vehicle control animals. High MCP1, IL-6, and eotaxin levels distinguished CloisNa-exposed animals from other treatments and are known to coincide with nanosized silica particle exposure in lung.[66] Compared to CloisNa, Clois30B exposure caused only 9 cytokines to significantly increase above controls. Notably, Clois30B still elicited significant increases in IL-6, MIP-1α, MIP-2, and TNFα but did not overexpress MCP1, MDC, eotaxin, OPN, TGFβ, or PDGF-bb. The absence of these cytokines compared to CloisNa samples indicated that mice exposed to ONC did not mount a strong day 1 inflammation recruitment signal, despite significantly elevated levels of TNFα, IL-6, MIP-1α, and MIP-2. These last four elevated cytokines did suggest moderate cellular damage, possibly from the QAC-based coating, since they are typically released by macrophages and damaged epithelial and fibroblast tissues.[67,68] I-Clois30B caused a similar expression profile to CS, with only MDC and eotaxin being specific for I-Clois30B. All other low-dose particle exposures caused significant 3.4- to 26-fold increases in MIP-1α only, while low-dose Clois30B caused 16-fold increased MMP9 expression (Supplemental Table 2).

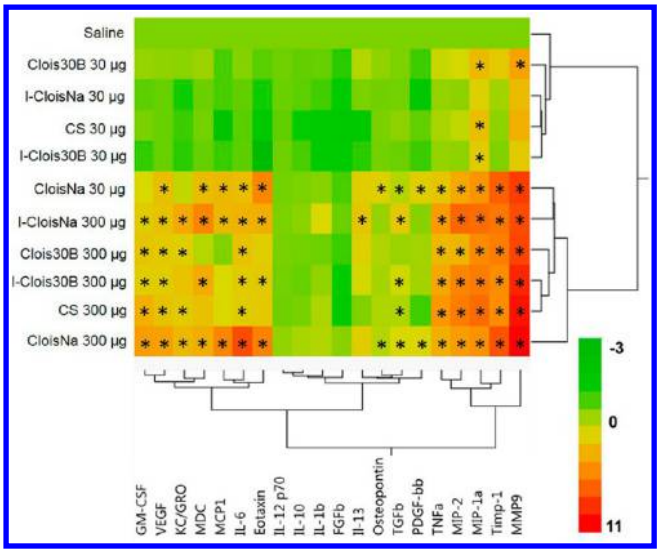

Figure 5. Heat map and hierarchical cluster analysis of BAL cytokine expression profiles at day 1 following pre- and post-incinerated organomodified nanoclay pulmonary exposure. Color scale bar represents Log2-fold change values. * indicate those treatments that were significantly different from their time-associated vehicle controls ($p < 0.05$, $n = 8$).

By day 7 postexposure, only high-dose CloisNa, Clois30B, and CS exhibited similar elevated inflammatory profiles compared to all other particle treatments and vehicle control animals (Figure 6a). Discriminant canonical analysis (DCA), however, indicated that these three exposures had distinct expression signature profiles (not shown). All three particles elicited significant 2.5- to 47-fold increases in inflammatory (TNFα, MIP-1α, MIP-2, MDC) and 1.8- to 124-fold increases in fibrosis-associated cytokines (OPN, MMP9, TIMP1, TGFβ), while ≥4-fold elevated PDGF-bb was specific for both nanoclays (Figure 6b). In addition, Clois30B retained significant 2.2-fold elevated levels of IL-6 and exhibited maximum peaks in MCP1, MDC, eotaxin, and TNFα expression suggesting prolonged tissue damage in airways (Figure 4). This, coupled with continued elevated cytotoxicity, suggested that persistent presence of the ONC particle elicited a delayed cytotoxic and pro-inflammatory signal response compared to pristine CloisNa, possibly due to slow dissolution of the QAC coating. Alternatively, CS exhibited overexpressed KC/GRO and decreased IL-12 and IL-13 expression. High-dose incinerated nanoclays (I-CloisNa and I-Clois30B) exhibited drastic 2.1- to 325-fold reductions in inflammatory cytokine expression compared to day 1 animals. All low-dose particle-exposed animals exhibited cytokine profiles similar to vehicle control animals.

On day 28 postexposure, high-dose I-Clois30B- and CS-exposed animals showed similar significantly elevated pro-inflammatory and fibrosis-associated cytokine expression profiles including several macrophage, neutrophil chemotactic, and extracellular matrix remodeling proteins (MMP9, TIMP1, and OPN; Figure 7a,b). Compared to other treatments, 1.6- to 16-fold elevated IL-6, MCP1, MDC, KC/GRO, eotaxin, and TNFα were specific to this group. MCP-1 is known as a potent promotor of inflammatory-driven fibrosis and is associated with autophagy following CS exposure.[69] Such a striking similarity between these treatments potentially suggested that incinerated ONCs may represent a chronic pulmonary hazard similar to

DOI: 10.1021/acsnano.7b07281
ACS Nano 2018, 12, 2292−2310

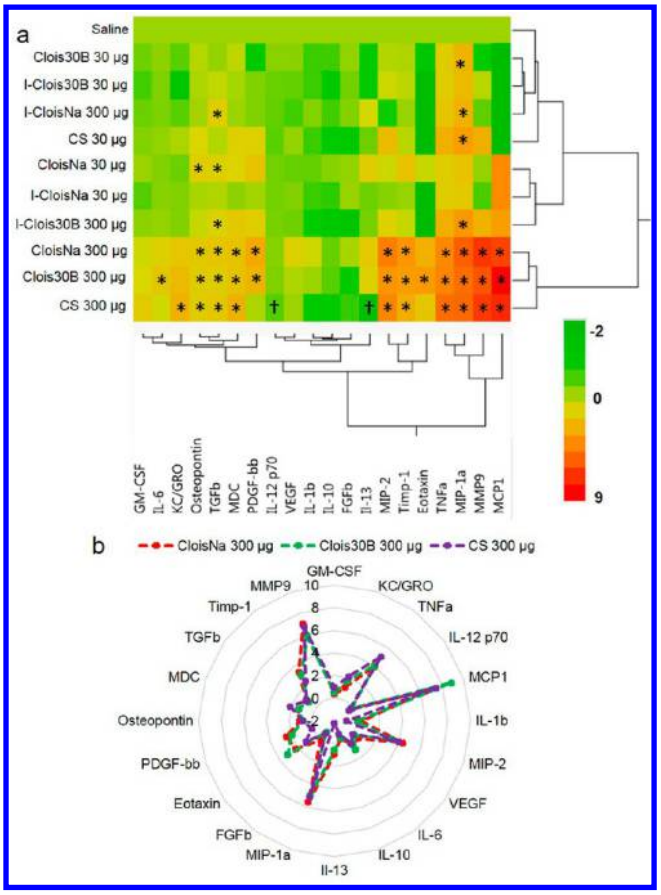

Figure 6. Hierarchical cluster analysis of BAL cytokine expression profiles at day 7 following pre- and post-incinerated organo-modified nanoclay pulmonary exposure. (a) Heat map and (b) radar plot depicting high-dose CloisNa, Clois30B, and CS with similar inflammatory and fibrotic tissue signaling profiles. Color scale bar represents Log2-fold change values. * indicate those treatments that were significantly different from their time-associated vehicle controls ($p < 0.05$, $n = 8$).

CS.[38,53,70] Although not as robust, both high-dose preincinerated nanoclays (CloisNa and Clois30B) caused a significant 1.5- to 40-fold elevation in fibrotic tissue profile, including clustered MIP-1α, MIP2, MMP9, PDGF, OPN, and TGFβ expression. DCA confirmed these two well-defined clusters of pro-inflammatory/fibrotic (I-Clois30B and CS) and low inflammation/fibrotic tissue (CloisNa and Clois30B) cytokine signatures. Of note, high-dose Clois30B exhibited a time-dependent increase in OPN from day 1 until peak at day 28, which matched high-dose CS animals. Persistent elevation of a fibrotic tissue BALF cytokine signature similar to CloisNa (TGFβ, OPN, PDGF, MIP2, and IL-6), coupled with elevated macrophage counts, particle-laden macrophages, and significant increase in binucleated macrophages suggests that ONC particle exhibits adverse effects on macrophages that may promote chronic disease development similar to uncoated montmorillonite, regardless of the absence of a robust acute inflammation response. IL-6 is not only involved in lung inflammation, but is a major contributor to asthma and COPD disease progression.[71] Binucleated macrophages could be the result of endosome trafficking disruption and improper trafficking of proteins involved in cytokinesis.[72] OPN is considered a regulator of inflammatory and fibrotic response and is associated with collagen III deposition, a major protein in reticular fiber, in mouse models.[73,74] Increasing evidence suggests that lung fibrosis and airway remodeling may still occur without a significant inflammatory presence.[75] Future research should identify whether ONC persistence and elevated fibrotic tissue cytokine signatures promote chronic, inflammatory-independent adverse lung pathology.

QAC Coating Reduced Lung Inflammation and Granuloma Severity Following Uncoated Nanoclay Exposure. The incidence and mean severity of pulmonary pathology is summarized in Table 3. The severity of lung pathology was dose-dependent for each particle examined, with the high dose eliciting more severe changes. In general, aspiration of CloisNa induced the most severe lung toxicity at both doses, when compared with the other particles examined. Specifically, inflammation following exposure to Clois30B, I-CloisNa, and I-Clois30B peaked at day 1 and resolved over time, whereas inflammation following CloisNa peaked at day 7 and persisted through the 28 day recovery period.

In high-dose CloisNa-exposed mouse lung, small numbers of neutrophils were seen at the TBs extending into the ADs and alveoli at day 1 postexposure (Figure 8 a2). Inflammatory cells were associated with deposition of abundant fine, grainy, bluish material (presumably nanoclay). The extent and severity of pulmonary inflammation was markedly increased at day 7 following exposure, with large, nodular aggregates of macrophages that effaced normal lung architecture (Figure 8 a3). Infiltrating macrophages were laden with a fine, grainy, bluish material (EDX confirmed Si and Al nanoclay signature; Figure 8 a3) similar to that observed at day 1. Inflammation tended to be centered at the TBs with extension into ADs and alveoli. Prominent pneumocyte hyperplasia and metaplasia near the TBs and ADs were clearly evident and were often seen within foci of pneumonia, occasionally forming tubular ductlike structures. At 28 days postexposure, prominent lymphoid nodules were found within foci of granulomatous inflammation (Figure 8 a4). Low-dose CloisNa-exposed animals showed similar pathology but less severe. On day 7 prominent Type II pneumocyte hyperplasia near the TBs and ADs was clearly evident. Alveolar Type II pneumocyte hyperplasia is a typical response to alveolar lipoproteinosis following exposure to damaging inorganic dusts, including crystalline silica and quartz.[14] The appearance of these macrophage and lymphocyte lesions with grainy montmorillonite deposits closely match those described in both previous *in vivo* and human epidemiological studies following occupational exposures to bentonite and Fuller's earth.[14,76] Montmorillonite lesions are typically characterized as particle laden with foamy protoplasm, carbohydrate-rich, reticular fibers, and little to no collagen deposition.[11,12,42] These foci typically possess low metabolic levels and storage ability over months to years indicating relatively low clearance.[12] Inhalation studies reported rapid, but transient clearance ability to the gastrointestinal tract, lymph nodes, and evidence of some dissolution in the lung,[77,78] with long-term clearance occurring primarily *via* mechanical or dissolution processes. Our high-dose CloisNa in a mouse (15 mg/kg) approximated a 5 mg/rat dose (~20 mg/kg) with similar deposition, inflammatory response, granulomas, and mild fibrosis with little increased collagen deposition.[42]

The organic coating of nanoclay (Clois30B) decreased the extent and severity of lung toxicity when compared to uncoated particles (CloisNa) (Figure 8a). At day 1 after Clois30B exposure, small numbers of neutrophils were seen at both TBs and ADs, often in association with aggregates of particles

DOI: 10.1021/acsnano.7b07281
ACS Nano 2018, 12, 2292–2310

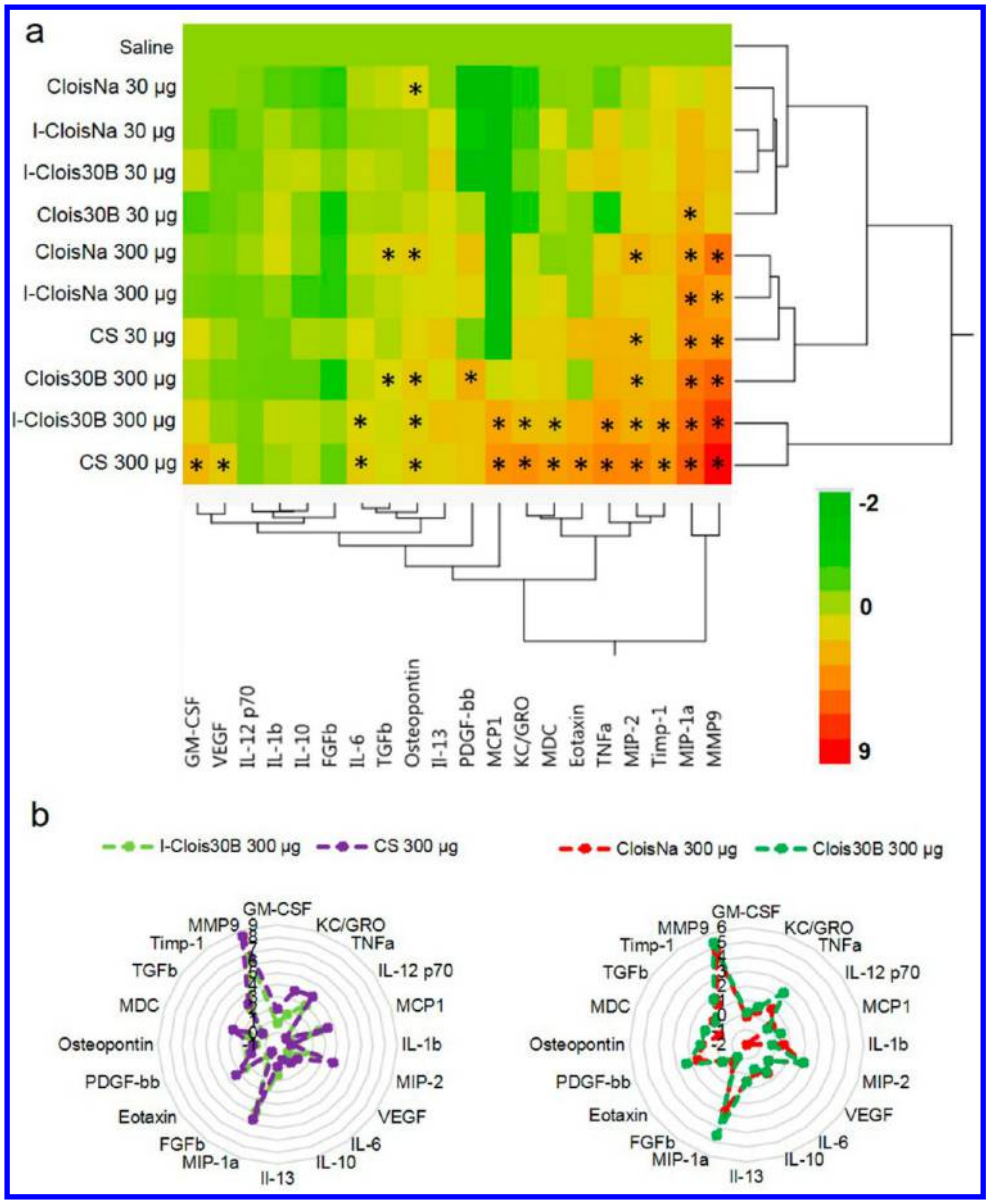

Figure 7. Hierarchical cluster analysis of BAL cytokine expression profiles at day 28 following pre- and post-incinerated organomodified nanoclay pulmonary exposure. (a) Heat map showing I-Clois30B and CS showing similar inflammatory profiles, while CloisNa and Clois30B showed similar fibrotic tissue signature profiles. Color scale bar represents Log2-fold change values. * indicate those treatments that were significantly different from their time-associated vehicle controls ($p < 0.05$, $n = 8$). (b) Radar plots depicting a more inflammatory (left) *vs* more fibrotic profiles (right).

Table 3. Incidence and Mean Severity of Lung Pathology[a,b]

		particle					
dose (μg)	day	saline	Clois Na	Clois 30B	I-Clois Na	I-Clois 30B	CS
30	1	0/4 (0.0)	4/4 (1.75)[c]	3/4 (0.75)	2/4 (0.5)	0/4 (0.0)	0/3 (0.0)
30	7	0/4 (0.0)	4/4 (2.25)[c]	1/4 (0.25)	0/4 (0.0)	0/4 (0.0)	0/4 (0.0)
30	28	1/4 (0.75)	3/4 (0.75)	0/4 (0.0)	0/4 (0.0)	0/4 (0.0)	0/4 (0.0)
300	1		4/4 (2.0)[c]	4/4 (1.5)[c]	4/4 (3.0)[c]	4/4 (2.25)[c]	4/4 (1.0)
300	7		4/4 (4.0)[c]	4/4 (1.5)[c]	4/4 (1.0)	2/4 (0.5)	4/4 (1.0)[c]
300	28		4/4 (3.0)[c]	3/4 (0.75)	1/4 (0.25)	2/4 (0.5)	3/4 (1.0)

[a]Incidence is stated as the number of positive animals out of $n = 4$ per group. [b]Average severity score in parentheses ranged from 0 to 4. [c]indicates significant increase in severity compared to saline controls using Fisher's exact test ($p < 0.05$).

(Figure 8 a5). This acute inflammation did not persist through the 28 day recovery period (Figure 8 a6 and a7). In day 7 and day 28 animals, Clois30B particulate was either engulfed or surrounded by alveolar macrophages (Supplemental Figure 4a, right panel). Exposure to both doses of CloisNa and high-dose Clois30B resulted in granulomas, first appearing at day 7

DOI: 10.1021/acsnano.7b07281
ACS Nano 2018, 12, 2292−2310

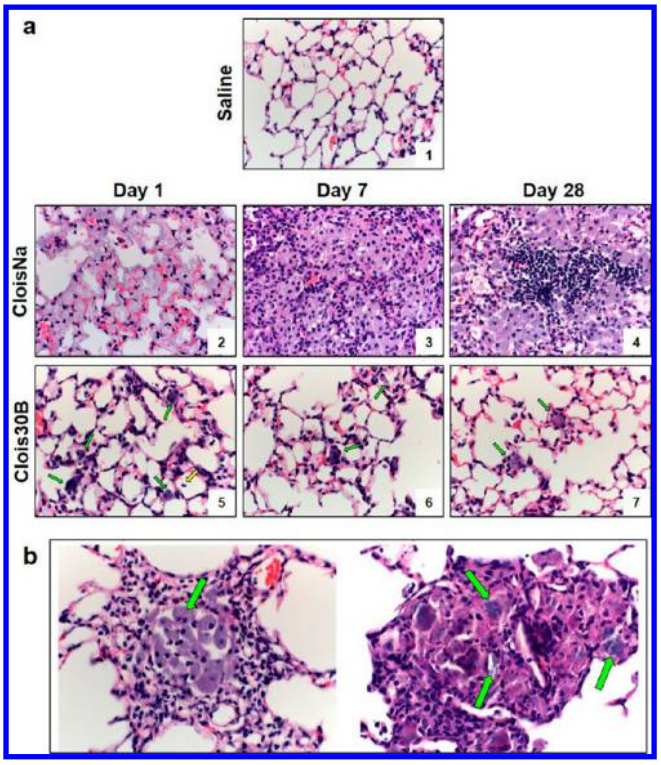

Figure 8. Time course of C57BL/6 male lung histopathology response following 300 μg aspiration exposure to pristine (CloisNa) or organomodified (Clois30B) montmorillonite nanoclay. CloisNa exposure (a) caused pulmonary edema on day 1 and robust neutrophil and macrophage inflammatory response that peaked at day 7 characterized by macrophage and type II pneuomocyte hyperplasia and focal lymphocyte infiltrate out to day 28. Conversely, Clois30B exposure resulted in mild neutrophilic inflammation associated with particle-laden macrophages. 400× magnification. Both CloisNa (b; left panel; day 28) and Clois30B (right panel; day 7) exposures caused granulomas comprised of macrophages and nanoclay particulate. 400× magnification. Blue and red arrows indicate free or macrophage engulfed particles, respectively.

postexposure, containing nanoclay particles (Figure 8b), which were more pronounced in CloisNa-exposed tissue. The marked reduction in pulmonary inflammation can possibly be attributed to the presence of the tallow coating. In efforts to improve dispersibility and safe-by-design ENMs, development and application of thin coatings has gained wide interest and implementation in nanotechnology[79] since they allow the ENM to retain its technological properties, and may shield exposed tissues from the surface properties of the raw ENM. Based on the ENM technological purpose, coatings can produce diminished or enhanced toxicological responses once exposed to tissues. Numerous studies report that organic polymer coatings reduce inflammation and membrane damage of the underlying raw ENM.[80,81]

In addition, cytokines and proteins associated with wound healing and extracellular matrix remodeling (OPN, TGFβ, TIMP1, MMP9, PDGF-bb) were elevated and coincided with prevalence of granulomas with some evidence of increased collagen deposition within the granuloma walls. Although not measured in this study, slow dissolution of the organic coating[31,80] either within the lung lining fluid or following macrophage phagocytosis could partially explain the delayed cytotoxicity, inflammatory, and fibrotic tissue signal until day 7. Inhalation exposure to some QAC compounds caused acute decreased tidal volume, reduced body weight, elevated MIP-2, IL-6, IgE, alveolar macrophage in the interstitium and focal aggregates, and mild lipoproteinosis.[82,83] Furthermore, several QAC compounds in nasal spray formulations are known to interfere with airway cilia beating.[84] This raises a question of whether dissolution of QAC-based coatings on ONCs slow mucociliary clearance resulting in persistence of deposited ONC and represents an area of future research. Increased deposition of extracellular matrix in the lung or within granulomas was minimal in this study out to day 28 postexposure. Nevertheless, resolution of a majority of the inflammatory signal by day 28, but retention of elevated fibrotic signaling, for both preincinerated nanoclays indicates several possibilities. First, regardless of initial acute inflammatory response, the persistence of each particle within the lung drives a fibrotic tissue cytokine signature associated with continued wound healing response. Second, prolonged pro-fibrotic signaling may promote increased fiber deposition and development of a collagen-poor, reticular fiber pathological response.[42] Prolonged elevated levels of fibrosis-associated cytokines, including those in the ONC signature, are known to promote several lung airway remodeling diseases including COPD, asthma, and fibrosis.[85−87] Reticular fiber reorganization can be observed in early stages of lung fibrosis.[88] Given the known chronicity of montmorillonite ECM lung pathology, a reticular fiber-associated lung remodeling may occur. Lastly, the fibrotic tissue signature will stay elevated until wound healing is complete and majority of the persistent particle has cleared the lung. Future studies may consider evaluating dose−response at longer postexposure time frames or repeated dosing given the recently reported high occupational exposure levels and a longer time frames for full development of montmorillonite-induced pathologies.

Incineration of uncoated CloisNa (I-CloisNa) altered both the type and kinetics of lung inflammation elicited upon exposure when compared to CloisNa. Pulmonary exposure to I-CloisNa resulted in a robust neutrophilic infiltrate at TBs at day 1, which resolved during the 28 day recovery period (Supplemental Figure 6). This is in contrast to CloisNa, which elicited a prominent granulomatous response at 7 days that persisted throughout the 28 day recovery period (Figure 8a). Exposure to high-dose I-Clois30B elicited an acute inflammatory response indistinguishable from that observed with exposure to I-CloisNa (Supplemental Figure 6) which resolved over time (Table 3). Exposure to high-dose CS induced minimal changes characterized by increased alveolar macrophages and few neutrophils surrounding the bronchioles, which persisted to day 28 (Supplemental Figure 6; Table 3). One of the most important factors in chronic development of pulmonary fibrosis is unresolved inflammation.[89] Lavagable PMNs are usually not the best predictor of fibrogenesis; rather, the inherent, prolonged inflammatory and known key signaling promotors are (*e.g.*, TGFβ). Occupational pulmonary exposure to CS results in silicosis, which is characterized by persistent levels of silica, inflammation, and collagen deposition in the lung.[13] Numerous rat inhalation studies report that the underlying mechanism is biphasic characterized by initial persistent inflammation with no enhanced collagen deposition, followed by rapid increases in inflammation, damage, and fibrosis.[51−53] Here, the CS was not freshly fractured, hence the absence of an acute inflammatory response.[90] The structure and reactive surface moieties of CS has been shown to cause

DOI: 10.1021/acsnano.7b07281
ACS Nano 2018, 12, 2292−2310

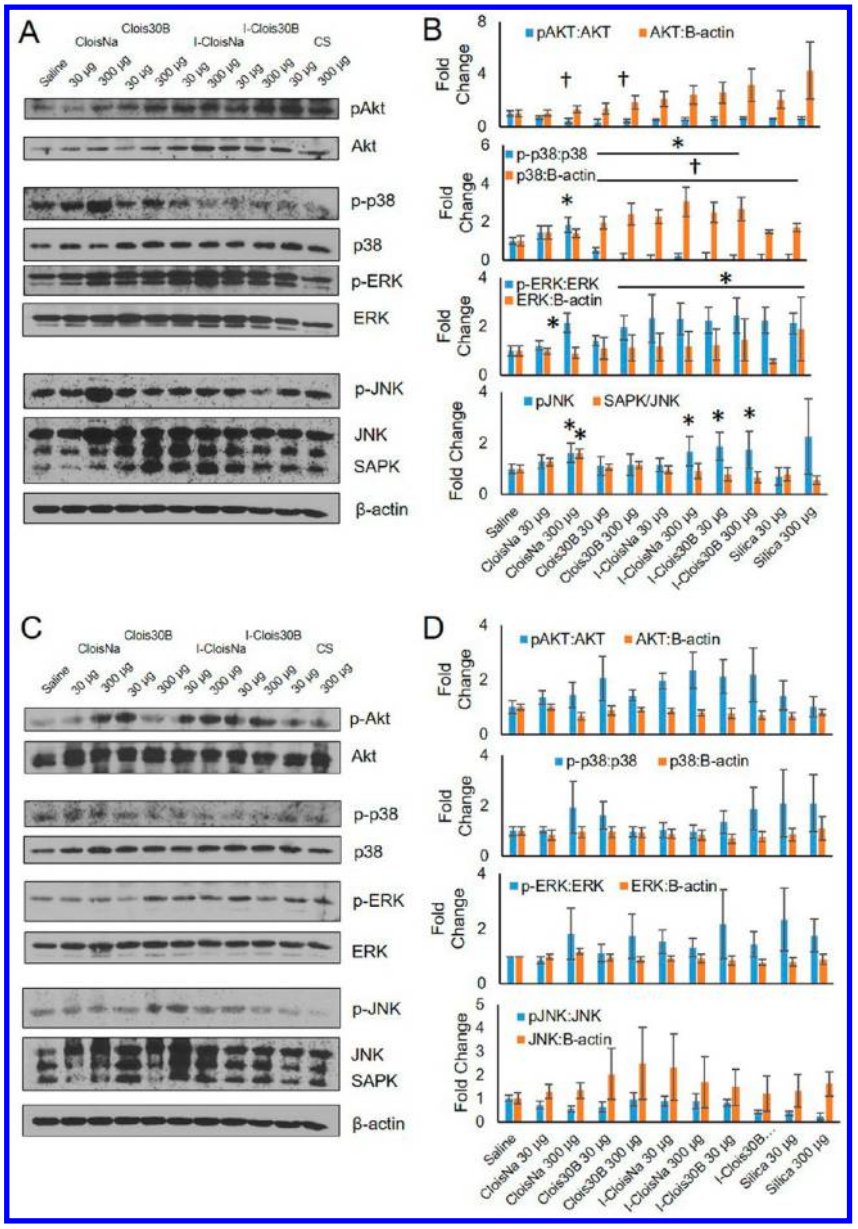

Figure 9. Akt, MAPK, and NFκB signaling at day 1 and day 7 following exposure to pre- and post-incinerated organomodified nanoclay. Western blot and quantitative densitometry analysis of protein bands at (a) and (b) day 1 and (c) and)d) day 7 postexposure. Phosphorylated and basal protein expression was normalized to basal and B-actin protein expression, respectively. * and † indicate significant increase or decrease, respectively, compared to saline-exposed animals ($n = 4$, $p \leq 0.05$).

membrane lysis and ROS, macrophage lysosome destabilization, and macrophage cytotoxicity, which promotes a persistent inflammatory response that can drive chronic lung fibrosis.[38] In general, fibrosis was not a prominent feature following exposure to any of the particles examined up to day 28. Minimal fibrosis was occasionally seen in the lung of high-dose CloisNa- and Clois30B-exposed animals associated with deposited particles in the noted granulomas (Figure 8b). In our model, CS appeared to elicit more tissue damage over time (*i.e.*, LDH and pathological score) and elevated neutrophil infiltrate at day 28 than I-Clois30B. Although no significant observable increase in collagen production in CS-exposed lung tissue was observed, this matches previous time course studies with similar doses in rat inhalation model where fibrosis was first identified at 40 d with 0.525 $\mu g/cm^2$ deposition.[51,52] Given future market projections of ONC production and disposal, future studies may consider evaluating the impact of longer recovery times following incinerated ONC exposure on pulmonary inflammation, tissue damage, and potential enhanced collagen deposition.

Differential Inflammatory Signaling in Whole Lung Associated with Coating and Incineration Status of Nanoclay. To investigate ONC-exposed lung inflammatory status, several key proteins in major inflammatory pathways were assessed. On day 1 postexposure, phosphorylated Akt (pAkt) was significantly downregulated 2.2-fold for high doses of both preincinerated nanoclays in exposed lung tissue. All other pAKt and basal Akt levels for other treatments showed no significant effect compared to saline-exposed animals (Figure 9a). pAkt serves as a cell survival response decreases downstream apoptotic signaling, and induces NFκB transcription following PDGF and TNFα activation,[91,92] thus

DOI: 10.1021/acsnano.7b07281
ACS Nano 2018, 12, 2292–2310

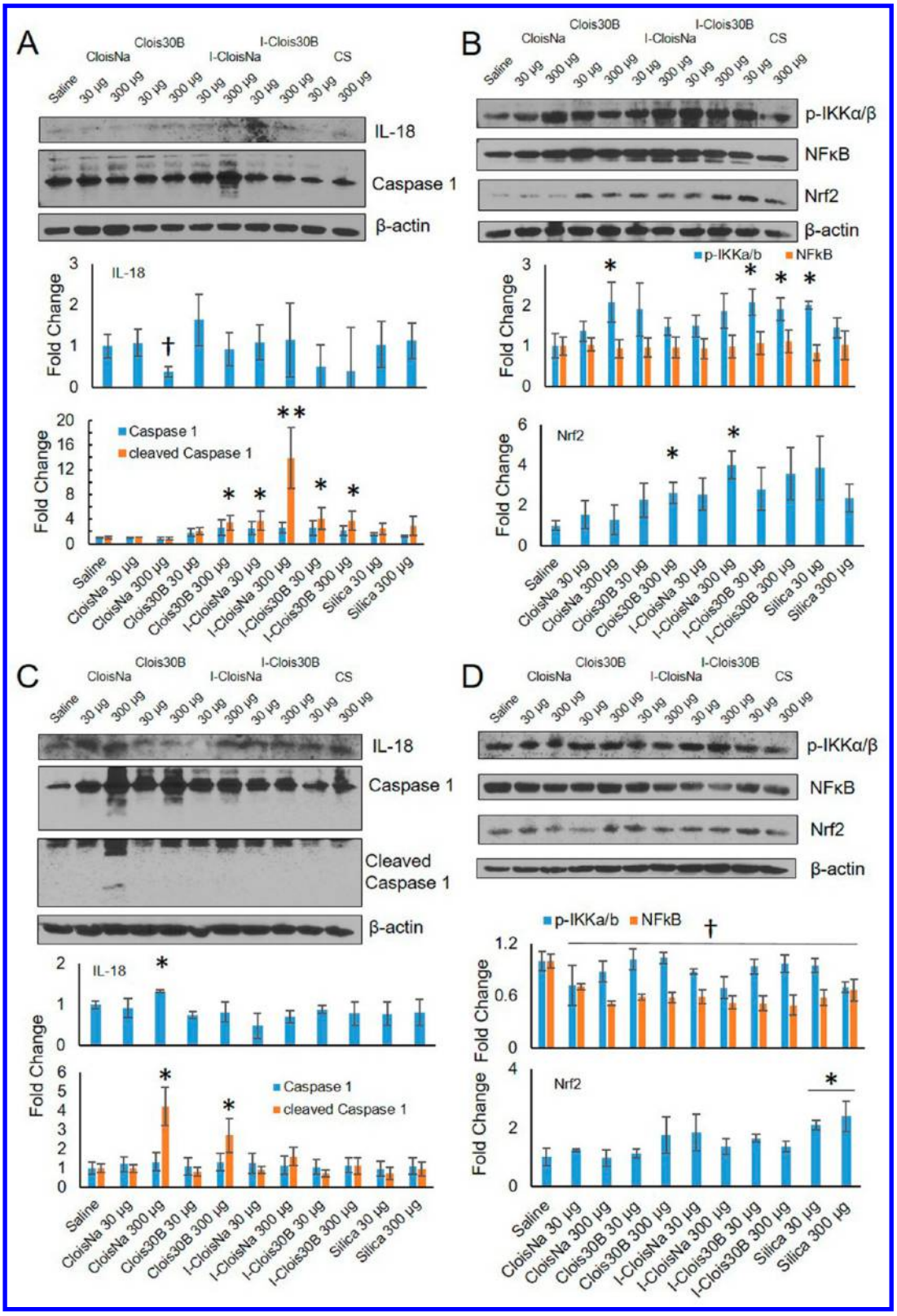

Figure 10. Caspase 1, IL-18, and NFκB signaling at day 1 and day 7 following exposure to pre- and post-incinerated organomodified nanoclay. Western blot and quantitative densitometry analysis of protein bands at (a) and (b) day 1 and (c) and (d) day 7 postexposure. Phosphorylated and basal protein expression was normalized to basal and B-actin protein expression, respectively. * and † indicate significant increase or decrease, respectively, compared to saline-exposed animals ($n = 4$, $p \leq 0.05$).

suggesting that high-dose nanoclay exposure reduced cell survival signaling and NFκB-mediated inflammatory induction. Next, activation of several members of the mitogen-activated protein kinase (MAPK) family were measured. High-dose CloisNa exposure resulted in significant increased activation ranging 1.6-to 2.1−fold of p38, ERK, and JNK indicating a

DOI: 10.1021/acsnano.7b07281
ACS Nano 2018, 12, 2292−2310

robust stress response in whole lung tissue. Only basal JNK levels were significantly elevated 1.6-fold in exposed high-dose CloisNa animals compared to all other treatments. These MAPK signaling pathways reside downstream of numerous overexpressed cytokines found in BALF, thus supporting a broad, robust stress and inflammatory response[93,94] and are consistent with previous reactive silica particle studies.[95,96] Conversely, low and high-dose of all other particles caused significant decreased phosphorylated p38 to almost undetectable levels compared to unexposed lung. Decreased p-p38 levels were shown to serve as a strong anti-inflammatory signal in a rat cardiopulmonary model,[97] thus suggesting that Clois30B and incinerated nanoclay exposure elicited an acute anti-inflammatory effect at day 1 postexposure. High-dose Clois30B, both doses of incinerated nanoclays, and both doses of CS significantly induced active ERK. Conversely, high-dose I-CloisNa and both doses of I-Clois30B exposure caused significant activation of JNK, indicating an inflammatory signal *via* JNK signaling pathway common for silica particles.[95]

At day 7 postexposure, moderate increases were observed for pAkt, p-p38, and pJNK in exposed lung; however, no particle treatments showed a significant difference in phosphorylated or basal Akt, MAPK, or JNK proteins compared to saline controls (Figure 9c and d, $p > 0.05$). These data are consistent with silica particle acute stimulation of stress and inflammatory signaling pathways with subsequent decrease over time. Acute silica nanoparticle exposure is known to activate p38 MAPK and NFkB signaling in both *in vitro* and *in vivo* models.[98,99] Conversely, larger particulate (*i.e.*, Clois30B and both incinerated clays) were able to elicit an anti-inflammatory response (decreased p-p38), which correlated with lower BALF inflammatory signature over the study's time course.

Damaging ultrafine particles can damage phagosome membranes in macrophages and epithelial cells resulting in NRLP3 inflammasome activation, caspase 1 cleavage and activation, and release of active pro-inflammatory IL-1β and IL-18.[100,101] On day 1 postexposure, caspase 1 cleavage was significantly increased 14-fold for high-dose I-Clois Na (Figure 10a) while modest significant increases (3.5- to 4-fold) were observed for high-dose Clois30B, low-dose I-CloisNa, and both doses of I-Clois30B compared to saline controls. High-dose CloisNa caused a significant decrease in IL-18 expression, while all other treatments showed no significant change compared to controls. Next, NFκB signaling is a major signaling axis contributing to inflammation, with IKKα/β serving as the key inhibitor complex in NFκB p65 activation. p-IKKα/β levels typically indicate IKKα/β degradation and predictive of NFκB p65 activation.[102] At day 1 postexposure, high-dose CloisNa, both doses of I-Clois30B, and low-dose CS caused 2-fold significant increases in p-IKKα/β. Whole lung NFκB p65 levels, however, remained unaltered compared to saline controls. Lastly, Nrf2, a key transcriptional regulator that promotes and controls several oxygen radical stress response enzymes and signaling,[103] was observed to significantly increase following high-dose Clois30B and I-CloisNa. All other treatments showed no effect compared to saline controls. These data suggest that high-dose I-CloisNa exposure induced inflammasome activation, NFκB activation, and antioxidant defense response. In addition, NFκB activation in high-dose CloisNa-exposed lung is consistent with day 1 BALF signature and a robust inflammatory response to a pyrogenic reactive silica particle.[38]

Coinciding with the day 7 delayed inflammatory response, cleaved Caspase 1 was significantly elevated 4.2- and 2.6-fold in CloisNa- and Clois30B-exposed lung, respectively. IL-18 levels were also significantly elevated 1.3-fold in CloisNa-, but not in Clois30B-exposed lung. With no evidence of altered IL-1β levels, our data suggests that both pristine and ONC exposure results in a delayed NRLP3 inflammasome response, evidenced by caspase 1 cleavage; however, only high-dose CloisNa induces a pro-inflammatory IL-18 signal. Next, no difference in p-IKKα/β levels were observed; however, all particle-exposed whole lung exhibited decreased NFκB expression compared to saline control. Only CS-exposed mice exhibited significantly elevated Nrf2 levels which is consistent with CS induction of ROS which promotes chronic inflammation.[51,52,70] NRLP3 inflammasome induction following pathogenic particle exposure relies on increased ion flux, reactive oxygen species, and/or lysosome rupture.[101] IL-1β and IL-18 release causes T-cell survival and activation, B-cell survival, and leukocyte migration through stimulation of other pathways to release other chemokines/cytokines including TGFβ, TNFα, and PDGF, which we observe in day 7 BALF fluid. In addition, caspase 1 activation is involved in pyroptosis, a cell death pathway involving necrosis and apoptosis.[104] Increasing evidence suggests that NRLP3 inflammasome activation, IL-1β family cytokine release, and pyroptosis in airway macrophages and epithelial cells promote COPD, fibrosis, and silicosis following silica particle exposure.[105,106] Our preliminary *in vitro* data show that Clois30B-exposed human macrophages exhibit Cathespin B release at subtoxic doses ($\geq$0.02 μg/cm^2) and cytotoxicity at *in vitro* doses just above this study's high dose on a mass per alveolar surface area dose metric ($\geq$2 μg/cm^2; data not shown). It appears that both high-dose preincinerated nanoclay produce a similar delayed caspase 1 activation until day 7 that correlates with similar pro-inflammatory and pro-fibrogenic BALF cytokine profile (Figure 6) and may partially explain the similar pro-fibrotic BALF signatures at day 28 postexposure. It remains unclear if macrophage and lung epithelial cell damage and death following ONC exposure is associated with caspase 1-dependent pyroptosis and is an area for future study.

Nanoclay Exposure Induced Acute Systemic Platelet Activation and Altered Systemic Leukocyte Populations. Platelet activation in exposed animals was time- and particle-dependent ($p < 0.0001$). All day 1 animals, except those exposed to high-dose I-CloisNa and low-dose I-Clois30B, exhibited significantly decreased time to clot, ranging −25% to −49%, in the tail bleed assay (Supplemental Figure 7). By day 7 postexposure, only low- and high-dose CloisNa- and high-dose CS-exposed animals retained significantly decreased clotting times compared to vehicle controls. Systemic platelet counts were significantly increased by 6.8% in day 1 postexposure animals (553×10^3/ml; $p < 0.05$) compared to other time points (518×10^3/ml) while dose and particle had no effect. Inhalation of $PM_{2.5}$, including submicron particulate matter, can cause extra-pulmonary signaling, systemic pro-thrombotic effects, and adverse cardiovascular effects.[107] Although relatively understudied following pulmonary particle exposures, recent evidence suggests that platelet function may play a role in not only the lung response to damage, but aberrant activation may also drive adverse cardiovascular and systemic responses.[108,109] Thus, high doses of pre- and post-incinerated ONC may pose cardiovascular risks in addition to lung injury.

Changes in total white blood cell (WBC) counts in whole blood collected from exposed animals, compared to vehicle-controls, was dose-, time-, and particle-dependent ($p = 0.049$;

DOI: 10.1021/acsnano.7b07281
ACS Nano 2018, 12, 2292−2310

Supplemental Figure 8a). Specifically, only low-dose Clois30B exhibited significantly suppressed WBC counts (−32% and −42%) at days 7 and 28. In addition, low-dose I-Clois30B, low-dose CS, and high-dose I-CloisNa possessed decreased counts, ranging −32 to −39%, at day 28. Evaluation of each major cell type showed inflammation-associated changes primarily at day 1 and evidence for immune suppression at day 28. Specifically, dose- and particle-dependent effects on systemic neutrophil counts in day 28 animals existed, which showed significantly suppressed neutrophil levels, ranging −49% to −54%, in low-dose Clois30B, I-Clois30B, and CS (Supplemental Figure 8b). In addition, high-dose I-CloisNa and CS exhibited reduced counts at day 28. Systemic neutrophil counts were significantly lower in day 7 and day 28 animals ($p < 0.0001$) compared to day 1 animals, possibly due to reduced neutrophil recruitment over time following acute pulmonary neutrophil infiltrate. Next, lymphocyte counts were dose-, particle-, and time-dependent ($p = 0.026$). High-dose CloisNa caused a significant decrease in lymphocyte counts on day 1 and day 28 (−47% and −29%, respectively), while low-dose CloisNa caused a 30% decrease in day 28 animals. These effects were mirrored by the robust lymphocytic infiltrate observed in sectioned lung tissue (Figure 8; Supplemental Figure 8c). Of note, a majority of exposed animals showed moderate, but significant lower lymphocyte counts, ranging −29% to −36%, at day 28, except for I-Clois30B and low-dose I-CloisNa.

Systemic eosinophil levels were dose-, time-, and particle-dependent ($p < 0.0001$). High-dose CloisNa exposure elicited a significant, dose-dependent decrease (−88%) in eosinophils at day 1 followed by a significant increase (100%) on day 7 compared to vehicle controls (Supplemental Figure 8d). This response was possibly due to large infiltrates into exposed lung tissue. All particle-exposed animals on day 28, except for low-dose CloisNa and high-dose I-CloisNa, exhibited significant decrease in eosinophils, ranging −45% to −58%, compared to vehicle-exposed animals. No differences were observed in monocyte blood counts of exposed animals versus vehicle-only controls (not shown). These data suggest that acute and low grade, persistent inflammatory response in the lung caused altered systemic blood cell populations in nanoclay-exposed mice. Although most exposed treatment groups showed near resolution of pulmonary inflammation at day 28 postexposure, the reduction in systemic eosinophil and lymphocyte counts, even for low-dose exposed groups, suggest that systemic impacts were still occurring. Reduced systemic counts of these two cell types imply potential immunosuppression or increased risk of cardiovascular disease.[110] Although this study focused on characterizing and comparing ONC exposure response in the lung, it is clear that potential systemic responses occurred well after a bolus-dose exposure and may signify an area of important research in the near future.

CONCLUSION

In summary, the presence of an organic modifier coating and incineration status of ONCs along their life cycle influences their inflammatory and tissue damage responses in exposed lung in the animal model. Hydrophobic coating of pristine montmorillonite resulted in reduced *in vivo* toxicity and histopathology in particle-exposed mice, possibly due to its polydispersity and larger particle size compared to well-dispersed, hydrophilic pristine montmorillonite. Persistence of preincinerated ONC particle in lung caused a low grade, delayed inflammatory response and tissue damage at day 7 resolving to a similar fibrotic tissue cytokine signature at day 28 to that of pristine montmorillonite. Conversely, incineration of the same particle resulted in a jagged morphological structure, which associated with a delayed pro-inflammatory cytokine profile, similar to crystalline silica. These data lend important pulmonary toxicological effect information for ONC occupational exposure and hazard along its product life cycle.

METHODS

Particle Characterization. Briefly, uncoated montmorillonite nanoclay Cloisite Na^+ (CloisNa) and organomodified nanoclay Cloisite 30B (Clois30B) were purchased from Southern Clay Products (Gonzales, TX). Clois30B possessed an outer methyl, tallow, bis-2-hydroxyethyl, quaternary ammonium coating at 90 mequiv/100 g clay. Min-U-Sil 5 crystalline silica (CS; U.S. Silica, Berkeley Springs, WV) was acquired and previously characterized as ≥98% quartz.[53] CS was chosen as an appropriate positive benchmark control given similar particle size and chemical makeup. Incineration of both nanoclays to produce I-CloisNa and I-Clois30B was conducted by thermogravimetric analysis (TGA701, LECO, St. Joseph, MI) up to 900 °C as previously described to evaluate particle composition and simulate municipal incineration.[36] All nanoclay samples were exposed to UV light for 30 min to reduce potential microbial contamination prior to *in vivo* exposure. Initial dry particle characterization on bulk prepared samples, including Fourier transform infrared spectroscopy (FTIR) and field emission scanning electron microscopy (FESEM) coupled with energy dispersive X-ray spectroscopy (EDX), was previously reported[36] to evaluate differences in surface groups on pre- and post-incinerated particles. These analyses indicated that UV exposure had no detectable effects on particle morphology or chemistry and that incineration completely removed all water and organic mass. Hence, UV-exposed particles were used for the entire study.

Since recent ONC exposure studies report nano and fine particle fractions either during manufacturing or in product manipulation,[9,10,26,111] we prepared dispersed particle stock solution to simulate these particle size distributions. Several milligrams of each test particle were placed inside a clean, endotoxin-free glass test tube with sterile USP water to achieve 12 mg/mL stock solutions. Next, each particle was dispersed *via* sonication in a water-immersed cup sonicator for 1 min per mL of stock solution at 40% intensity using Vibra-Cell 500 (Sonics and Materials Inc., Newtown, CT). Initial DLS analyses with different sonication durations was performed to ascertain the critical sonication energy delivered to achieve relatively stable dispersed particle suspensions.[112] DLS and zeta potential of freshly dispersed particles at 50 μg/mL were conducted on a Zetasizer ZS (Malvern Instruments, Westboro, MA) using a dip cell within 1 min following sonication in 0.9% pharmaceutical grade saline, the aspiration vehicle. To understand potential changes in particle dispersion once in contact with lung surfactant, separate stock solutions in water with 150 μg/mL Survanta, a natural lung surfactant, were prepared and briefly sonicated using previously described methods.[113]

FESEM and EDX morphological and chemical surface analyses of dispersed particles were conducted as previously described.[113,114] Briefly, freshly dispersed nanoclay and CS samples in water, saline, and lung surfactant were diluted to 1 μg/mL in an aspiration vehicle, filtered onto a polycarbonate filter (Millipore, Billerica, MA), dried, mounted, gold/palladium sputter coated, and imaged with a S-4800 FESEM (Hitachi, Tokyo) coupled with EDX (PGT Inc., Princeton, NJ). Based on DLS and FESEM particle morphology data showing exfoliated platelets, estimates for platelet aerodynamic diameter (D_{ae}) were calculated on the basis of previous methodology[49] using particle density, varied platelet thickness, and particle diameter size fractions from DLS analysis.

Endotoxin concentration in prepared particle stock solutions was assayed using a commercial Limulus amebocyte lysate kit (QCL-1000, Lonza, Walkersville, MD) using the manufacturer's and previously described methods.[115] Briefly, freshly suspended and dispersed particles in water (100 μg/mL) were shaken in endotoxin-free glass test tubes for 10 min to extract endotoxin from samples (ISO 29701).

DOI: 10.1021/acsnano.7b07281
ACS Nano 2018, 12, 2292−2310

Samples were centrifuged to pellet particulate, and then the supernatant was diluted to 1−100 μg/mL, plated into a 96-well plate in triplicate, incubated at 37 °C, and assayed for endotoxin at absorbance of 405 nm. An internal positive LPS spike was supplied to an extra 10 μg/mL sample to validate assay performance and ascertain nanoclay ability to adsorb LPS. Background blank values were subtracted from all data to assess particle-associated endotoxin.

Animal Care. Three week old male C57BL\6J mice (n = 396) were purchased from Jackson Laboratories (Bar Harbor, ME). Mice were group housed in Thoren Weaning cages with Harlan 7090C SaniChip bedding for 3 weeks with three mice per cage supplied with filtered HEPA air to acclimate animals to both laboratory and group housing conditions. Mice were closely monitored for evidence of fighting or lack of food access due to group housing for the study's duration. All animals were provided Harlan 7913 irradiated NIH-31 modified 6% feed and water *ad libitum* in temperature- and humidity-controlled animal quarters with a 12:12 light/dark cycle. The NIOSH Health Effects Laboratory Division Institutional Animal Care and Use Committee, which is AAALAC accredited, approved the study.

Study Design and Exposure. Six week old mice were exposed *via* oropharyngeal aspiration to either low (30 μg) or high (300 μg) dose per mouse for each of the five particles. Prior to the main exposure study, a pilot dose-range finding study was conducted with CloisNa and Clois30B at 0, 10, 100, and 1000 μg/mouse to ascertain doses for the large study using inflammatory response and airway damage end points at day 7. Low and high doses were chosen based on comparable deposited crystalline silica doses in rat inhalation studies.[53] Maximum CS dose for a 60 d inhalation exposure was 2.8 mg/rat lung, which equals 0.7 μg/cm^2 lung alveolar surface. The 30 and 300 μg bolus dose in a mouse lung with 500 cm^2 surface area gives a 0.06 and 0.6 μg/cm^2 dose, respectively. A randomized 3 × 5 × 3 block design with four blocks was used with 12 animals per treatment group. Each cage per block was randomly assigned to a treatment group. Briefly, one at a time, each particle stock solution was sonicated, immediately diluted in pharmaceutical grade saline vehicle to the reported dose, briefly vortexed, and administered to each treatment group. This was done to keep polydisperse particles and self-agglomeration to a minimum. Mice were anesthetized with isoflurane (Abbott Laboratories, Chicago, IL) and suspended by their two front incisors on a board. The tongue was gently held with forceps while 50 μL of dispersed particle was placed on the back of the tongue. Sham control mice received 50 μL of vehicle only. Mice were allowed to aspirate twice, placed on a scale to obtain initial body weights, and placed on their left side in their cage to regain consciousness. All exposed mice were monitored for the first 4 h and again at 12 h for signs of lethargy and stress.

Blood, BAL Fluid, and Tissue Collection. On days 1, 7, and 28 postexposure, each mouse was removed from their cage and gently restrained, and their tail was nicked with a sharp scalpel to measure time to clot as a measure of platelet activation following nanoclay exposure. Next, a subset of mice (n = 8) were anesthetized with isoflurane until last breath in a bell jar. Immediately following last breath, mice were weighed and then blood collected *via* cardiac puncture with an acid citrate−dextrose (ACD; Sigma-Aldrich, St. Louis, MO) filled needle tip to avoid platelet activation and clotting. Each blood sample was placed into Bio-one tubes (Greiner) containing 70 μL of ACD and set on ice. A 50 μL aliquot of whole blood from each sample was used for blood cell differential analysis on a ProCyte Dx (IDEXX Laboratories, Westbrook, ME). All blood samples were spun at 250 g for 15 min at 25 °C and 3.2k RPMs for 5 min to obtain platelet and platelet-poor plasma fractions, respectively. Each fraction was carefully removed *via* pipet, placed into small Eppendorf tubes, and frozen at −80 °C for future analyses.

Immediately following blood collection, each mouse underwent bilateral thoracotomy and prepared for BAL fluid collection. Briefly, a small nick in the trachea was made followed by insertion of a secured, sterile cannula. Next, 0.8 mL of sterile, cold phosphate-buffered saline (PBS; ThermoFisher, Grand Island, NY) was injected into the airways. The first lavage was collected and placed on ice in small Eppendorf tubes. Samples were spun at 1500 rpm for 5 min to pellet all cells and particles. Supernatants were removed, placed in a separate tube, and immediately frozen at −80 °C for airway damage marker and cytokine analyses. Three more lavages of 0.8 mL PBS were performed, collected, and pooled in a chilled 15 mL conical tube for cell differential analysis. Cell pellets from the first lavage were resuspended in a small volume of PBS and combined with pooled lavages. BAL cells were collected by centrifuging all samples at 1500 rpm for 5 min, aspirating supernatant, and resuspending cells in 250 μL of chilled PBS. Fifty microliter portions of sample were placed in cups with 20 mL of isotone and analyzed for cell counts and sizing *via* MultiCounter 4e (Beckman Coulter, Brea, CA). On the basis of the large amounts of particulate, airway damage, and cytotoxicity present in some samples,[116] all BALF live cell counts were performed *via* trypan blue staining on a Countess Automated Cell Counter (ThermoFisher) and manually spot checked on a hemocytometer. Lastly, appropriate volumes containing 1 × 10^4 cells were placed into centrifuge funnels holding glass slides and centrifuged at 800 g for 5 min to cytospin fix BAL cells. All slides were air-dried, fixed, and stained using HEMA 3 Giemsa staining kit (Fisher Scientific, Pittsburgh, PA). Cells were viewed under bright field microscopy and cell types determined for each sample (>300 cells per slide).

The remaining subset of mice (n = 4) were euthanized with intraperitoneal injection of ≥100 mg/kg of sodium pentobarbital followed by exsanguination. Briefly, the lungs were tied off at the first bifurcation with the left lung lobe being removed and immediately frozen at −80 °C for future protein analysis. The remaining right lung lobe was inflated with 10% buffered formalin and placed in a formalin-filled container with the tracheobronchial lymph nodes, liver, and kidney for current and future histopathological analyses. Briefly, tissues were allowed to formalin fix, paraffin processed, and embedded. Right lung 5 μm sections were prepared for hematoxylin and eosin (H & E), Picrosirius red (PSR), and Masson trichrome staining.

BAL Airway Damage, Cell Differential, and Proteomic analyses. First lavage supernatants were assayed for lactose dehydrogenase (LDH) activity by monitoring NAD^+ reduction during lactate conversion to pyruvate (Roche), and total protein levels with BCA kit (ThermoScientific) in triplicate, respectively, using manufacturers' protocols. Since ONC exposure effects on lung airway cytokine signaling is unknown, collected frozen BALF samples from 100 μg dosed mice from the small pilot study (n = 4) were shipped on dry ice to Ampersand Biosciences (Saranac Lake, NY) and subjected to a 42 multianalyte cytokine screening array (RodentMap 4.0). Based on these results, a smaller 17 target cytokine magnetic Luminex bead array (R & D Systems, Minneapolis, MN) was designed (Supplemental Table 1) and used to assay all collected BAL samples from the large animal study following manufacturer's protocol. In addition, TGFβ, MDC, and TIMP1 duoset or quantikine ELISA assays were conducted based following manufacturer's protocol (R & D Systems). Samples for TGFβ analysis were hydrochloric acid activated and neutralized prior to detection antibody incubation. All bead and ELISA assays were conducted on neat samples. Next, all cytokine concentrations were converted to Log_2 fold change based on vehicle control concentrations, and subjected to unsupervised hierarchical cluster analysis using Ward's method in JMP 12.0 (SAS, Cary, NC) to identify similar inflammatory expression profiles among particle exposures over time. Clusters were validated using discriminant canonical analysis. Fold change and p-value data (see below) for each cytokine compared to sham control was uploaded into Ingenuity Pathway Analysis (IPA, Qiagen, Redwood City, CA) to identify differences among groups in major pulmonary airway signaling responses. Core Analysis, using 1.5-fold criteria compared to vehicle controls followed by comparison analyses, were conducted in IPA.

Histopathology Scoring. H & E slides were scored by a veterinarian for overall extent and severity of inflammation, airway damage, and early signs of lung disease. Stained slides were examined using polarized light and enhanced dark field imaging (CytoViva, Auburn, AL) for visualizing particles (H & E) and collagen (PSR). Due to CloisNa's well-dispersed, platelet morphology, uncoated serial lung sections were evaluated by FESEM/EDX to identify deposited nanoclay in the lung. Severity of the histopathology was graded on a 5-point scoring system according to the following parameters: 0 = within

DOI: 10.1021/acsnano.7b07281
ACS Nano 2018, 12, 2292−2310

normal limits, 1 = minimal, 2 = mild, 3 = moderate, 4 = severe. Images were capture using an Olympus BX53 microscope equipped with a DP73 camera.

Western Blot Analyses. To investigate differences in inflammatory signaling, expression of several different key proteins in major inflammatory pathways were measured. Lung tissue preparation and Western Blot analysis were performed according to previously described methods.[113] Briefly, frozen whole lung samples were thawed on ice and placed into lysis tubes containing beads and ice cold RIPA buffer with sodium vanadate, PMSF, and protease inhibitor cocktail. Lungs were lysed with a FastPrep system (MP Biomedicals, Santa Ana, CA). Lysed samples were centrifuged at 2000 rpm, supernatants collected, and aliquoted. Samples were centrifuged at 12,000 rpm for 15 min followed by protein concentration determination by bicinchoninic acid assay (ThermoFisher Scientific, Grand Island, NY) according to manufacturer's directions. All primary antibodies were acquired from Cell Signaling Technologies (Danvers, MA), except for IL-18 and caspase 1, which were acquired from Abcam (Cambridge, MA). A 35 μg portion of protein was separated by 10% or 12% sodium dodecyl sulfate−polyacrylamide gel electrophoresis followed by transfer to nitrocellulose membranes *via* a semidry transfer apparatus (Fisher Scientific). Membranes were blocked in 0.5% nonfat dry milk in Tris-buffered saline with 1% Tween 20 and probed with primary and HRP secondary antibodies (Santa Cruz Technologies, Santa Cruz, CA) using an iBlot system (Millipore, Burlington, MA). Protein bands were visualized with incubation with Immuno (Millipore) or SuperSignal Femto (ThermoFisher Scientific) and film exposure. Films were digitally scanned and densitometry performed in ImageJ. Phosphorylated proteins were compared to their basal protein expression, while all other proteins were compared to β-actin (Sigma-Aldrich).

Statistics. Percent change in animal weight was calculated by subtracting final from initial divided by initial. All BALF data were calculated to determine means ± standard error (SE) followed by multifactorial analysis of variance (ANOVA) tests to compare among treatment groups. All data were log- or square-root transformed and residuals tested for normal distribution and homoscedasticity to meet ANOVA assumptions. For those results showing significant differences, either Tukey-Kramer HSD or Dunnett's tests were employed to identify significant treatment groups. Log 2 fold change and *p*-values were calculated for all cytokine treatments compared to sham control for hierarchical cluster and ingenuity pathway analyses (IPA). Since histopathological scoring was categorical, Fisher's exact test was used to identify significant differences. All statistical analyses were performed using JMP 12.0 with $\alpha = 0.05$.

ASSOCIATED CONTENT

Supporting Information

The Supporting Information is available free of charge on the ACS Publications website at DOI: 10.1021/acsnano.7b07281.

Supporting figures and legends (PDF)

Supporting tables containing BALF multiplex cytokine fold change data (PDF)

AUTHOR INFORMATION

Corresponding Author

*E-mail: tstueckle@cdc.gov. Tel: 304 285-6098.

ORCID

Todd A. Stueckle: 0000-0002-2495-7443

Cerasela Zoica Dinu: 0000-0002-6474-6771

Konstantinos A. Sierros: 0000-0002-6984-6376

Author Contributions

T.A.S., D.C.D., R.D., and L.W. participated in all aspects of this study including conception, experimental design, animal handling and exposure, tissue collection, analyses, and drafting the manuscript. T.G.K., L.B., S.F., and M.S.O. assisted with particle preparation and characterization, tissue collection, data analysis, and manuscript editing. A.W., K.S., and S.A. provided material generation and characterization. R.G., C.Z.D., Y.R., and D.W.P. participated in study conception, experimental design, expert advice, and drafting the manuscript. All authors have read and approved the final manuscript.

Funding

This study was supported by grants from the Nanotoxicology Research Center (FY16 JUX5), National Science Foundation (NSF) Grant Nos. 1434503 and 1454230, and the National Institutes of Health (ES022968). R.G. was funded by a grant from the King Abdulaziz City for Science and Technology (Riyadh, Saudi Arabia).

Notes

The findings and conclusions in this article are those of the authors and do not necessarily represent the view of the National Institute for Occupational Safety and Health. Mention of product names does not constitute endorsement. All animal procedures followed USDA and OLAW standards. The study was approved by the NIOSH IACUC.

The authors declare no competing financial interest.

ACKNOWLEDGMENTS

Thanks to M. Kashon in assisting with initial statistical power analyses for experimental design. We acknowledge use of WVU Shared Research Facilities and the WVU Analytical Lab.

REFERENCES

(1) Patel, H. A.; Somani, R. S.; Bajaj, H. C.; Jasra, R. V. Nanoclays for Polymer Nanocomposites, Paints, Inks, Greases and Cosmetics Formulations, Drug Delivery Vehicle and Waste Water Treatment. *Bull. Mater. Sci.* **2006**, *29*, 133−145.

(2) Carretero, M. I.; Gomes, C. S. F.; Tateo, F. Chapter 11.5 Clays and Human Health. *Dev. Clay Sci.* **2006**, *1*, 717−741.

(3) Anandhan, S.; Bandyopadhyay, S. Polymer Nanocomposites: From Synthesis to Applications. In *Nanocomposites and polymers with analytical methods*; Cuppoletti, J., Ed.; InTechOpen, 2011; pp 1−27.

(4) Camargo, P. H. C.; Satyanarayana, K. G.; Wypych, F. Nanocomposites: Synthesis, Structure, Properties and New Application Opportunities. *Mater. Res.* **2009**, *12*, 1−39.

(5) Mackevica, A.; Foss Hansen, S. Release of Nanomaterials from Solid Nanocomposites and Consumer Exposure Assessment- A Forward-Looking Review. *Nanotoxicology* **2016**, *10*, 641−653.

(6) Maisanaba, S.; Pichardo, S.; Puerto, M.; Gutierrez-Praena, D.; Camean, A. M.; Jos, A. Toxicological Evaluation of Clay Minerals and Derived Nanocomposites: A Review. *Environ. Res.* **2015**, *138*, 233−254.

(7) Floody, M. C.; Theng, B. K. G.; Mora, M. L. Natural Nanoclays: Applications and Future Trends: A Chilean Perspective. *Clay Miner.* **2009**, *44*, 161−176.

(8) Utracki, L. A., Wilkie, C., Eds. *Polymer Blends Handbook*; Springer: Netherlands, 2014.

(9) Tsai, S. J.; Ashter, A.; Ada, E.; Mead, J.; Barry, C.; Ellenbecker, M. J. Airborne Nanoparticle Release Associated with the Compounding of Nanocomposites Using Nanoalumina as Fillers. *Aerosol Air Qual. Res.* **2008**, *8*, 160−177.

(10) Tsai, C. S. J.; White, D.; Rodriguez, H.; Munoz, C. E.; Huang, C. Y.; Tsai, C. J.; Barry, C.; Ellenbecker, M. J. Exposure Assessment and Engineering Control Strategies for Airborne Nanoparticles: An Application to Emissions from Nanocomposite Compounding Processes. *J. Nanopart. Res.* **2012**, *14*, 989.

(11) Timár, M.; Kendrey, G.; Juhasz, Z. Experimental Observations Concerning the Effects of Mineral Dust to Pulmonary Tissue. *Med. Lav.* **1966**, *57*, 1−9.

DOI: 10.1021/acsnano.7b07281
ACS Nano 2018, 12, 2292−2310

(12) Ungváry, G.; Timár, M.; Tátrai, E.; Bacsy, E.; Gaal, G. Analysis of Aluminum Silicate Storage Foci in the Lungs. *Exp. Pathol.* **1983**, *23*, 203−214.
(13) IARC. Silica. IARC Monographs on the Evaluation of Carcinogenic Risks to Humans. *Silica, Some Silicates, Coal Dust and Para-Aramid Fibrils*; IARC Press: Lyon, France, 1997; Vol. *68*, pp 41−242.
(14) Adamis, Z.; Williams, R. B. Bentonite, Kaolin and Selected Clay Minerals. *Environmental Health Criteria 231*; World Health Organization: Geneva, 2005; p 175.
(15) Arora, A.; Padua, G. W. Review: Nanocomposites in Food Packaging. *J. Food Sci.* **2010**, *75*, 43−49.
(16) Souza, P. M. S.; Morales, A. R.; Marin-Morales, M. A.; Mei, L. H. I. PLA and Montmorillonite Nanocomposites: Properties, Biodegradation and Potential Toxicity. *J. Polym. Environ.* **2013**, *21*, 738−759.
(17) Hischier, R.; Walser, T. Life Cycle Assessment of Engineered Nanomaterials: State of the Art and Strategies to Overcome Existing Gaps. *Sci. Total Environ.* **2012**, *425*, 271−282.
(18) Mitrano, D. M.; Motellier, S.; Clavaguera, S.; Nowack, B. Review of Nanomaterial Aging and Transformations through the Life Cycle of Nano-Enhanced Products. *Environ. Int.* **2015**, *77*, 132−147.
(19) Transparency Market Research. *Nanoclay (Kaolinite, Smectite, And Others) Market for Packaging, Flame Retardants, Automotive, Paints & Coatings, and Other End-Users - Global Industry Analysis, Size, Share, Growth, Trends and Forecast 2015−2023*; Transparency Market Research, 2015; pp 171.
(20) Alateyah, A. I.; Dhakal, H. N.; Zhang, Z. Y. Processing, Properties, and Applications of Polymer Nanocomposites Based on Layered Silicates: A Review. *Adv. Polym. Technol.* **2013**, *32*, 21368.
(21) Murariu, M.; Dubois, P. PLA Composites: From Production to Properties. *Adv. Drug Delivery Rev.* **2016**, *107*, 17−46.
(22) Roes, A. L.; Marsili, E.; Nieuwlaar, E.; Patel, M. K. Environmental and Cost Assessment of a Polypropylene Nanocomposite. *J. Polym. Environ.* **2007**, *15*, 212−226.
(23) Zeng, S. L. Y. Z.; Zhang, Q. F.; Du, Y. J.; Sun, Y. T.; Zhang, M. J. Study on Occupational Standard of Bentonite Dust in Air of Workplace. *Zhonghua Laodong Weisheng Zhiyebing Zazhi* **1998**, *16*, 177−178.
(24) Huang, Y.; Zhang, M.; Zou, H.; Li, X.; Xing, M.; Fang, X.; He, J. Genetic Damage and Lipid Peroxidation in Workers Occupationally Exposed to Organic Bentonite Particles. *Mutat. Res., Genet. Toxicol. Environ. Mutagen.* **2013**, *751*, 40−44.
(25) Sachse, S.; Irfan, A.; Zhu, H.; Njuguna, J. Morphology Studies of Nanodust Generated from Polyurethane/Nanoclay Nanofoams Following Mechanical Fracture. *J. Nanostruct Polym. Nanocomp.* **2011**, *7*, 5−9.
(26) O'Shaughnessy, P. T.; Kang, M.; Ellickson, D. A Novel Device for Measuring Respirable Dustiness Using Low Mass Powder Samples. *J. Occup. Environ. Hyg.* **2012**, *9*, 129−139.
(27) Debia, M.; Bakhiyi, B.; Ostiguy, C.; Verbeek, J. H.; Brouwer, D. H.; Murashov, V. A Systematic Review of Reported Exposure to Engineered Nanomaterials. *Ann. Occup. Hyg.* **2016**, *60*, 916−935.
(28) Buha, J.; Mueller, N.; Nowack, B.; Ulrich, A.; Losert, S.; Wang, J. Physical and Chemical Characterization of Fly Ashes from Swiss Waste Incineration Plants and Determination of the Ash Fraction in the Nanometer Range. *Environ. Sci. Technol.* **2014**, *48*, 4765−4773.
(29) Holder, A. L.; Vejerano, E. P.; Zhou, X.; Marr, L. C. Nanomaterial Disposal by Incineration. *Environ. Sci: Processes Impacts* **2013**, *15*, 1652.
(30) Sotiriou, G. A.; Singh, D.; Zhang, F.; Chalbot, M. C. G.; Spielman-Sun, E.; Hoering, L.; Kavouras, I. G.; Lowry, G. V.; Wohlleben, W.; Demokritou, P. Thermal Decomposition of Nano-Enabled Thermoplastics: Possible Environmental Health and Safety Implications. *J. Hazard. Mater.* **2016**, *305*, 87−95.
(31) Janer, G.; Fernández-Rosas, E.; Mas del Molino, E.; González-Gálvez, D.; Vilar, G.; López-Iglesias, C.; Ermini, V.; Vázquez-Campos, S. *In Vitro* Toxicity of Functionalized Nanoclays Is Mainly Driven by the Presence of Organic Modifiers. *Nanotoxicology* **2014**, *8*, 279−294.
(32) Maisanaba, S.; Puerto, M.; Pichardo, S.; Jordá, M.; Moreno, F. J.; Aucejo, S.; Jos, Á. *In Vitro* Toxicological Assessment of Clays for Their Use in Food Packaging Applications. *Food Chem. Toxicol.* **2013**, *57*, 266−275.
(33) Maisanaba, S.; Hercog, K.; Ortuño, N.; Jos, Á.; Žegura, B. Induction of Micronuclei and Alteration of Gene Expression by an Organomodified Clay in HEPG2 Cells. *Chemosphere* **2016**, *154*, 240−248.
(34) Miller, B. G.; Hagen, S.; Love, R. G.; Soutar, C. A.; Cowie, H. A.; Kidd, M. W.; Robertson, A. Risks of Silicosis in Coalworkers Exposed to Unusual Concentrations of Respirable Quartz. *Occup. Environ. Med.* **1998**, *55*, 52−58.
(35) Hnizdo, E.; Vallyathan, V. Chronic Obstructive Pulmonary Disease due to Occupational Exposure to Silica Dust: A Review of Epidemiological and Pathological Evidence. *Occup. Environ. Med.* **2003**, *60*, 237−243.
(36) Wagner, A.; Eldawud, R.; White, A.; Agarwal, S.; Stueckle, T. A.; Sierros, K. A.; Rojanasakul, Y.; Gupta, R. K.; Dinu, C. Z. Toxicity Evaluations of Nanoclays and Thermally Degraded Byproducts Through Spectroscopical and Microscopical Approaches. *Biochim. Biophys. Acta, Gen. Subj.* **2017**, *1861*, 3406−3415.
(37) Wagner, A.; White, A. P.; Stueckle, T. A.; Banerjee, D.; Sierros, K. A.; Rojanasakul, Y.; Agarwal, S.; Gupta, R. K.; Dinu, C. Z. Early Assessment and Correlations of Nanoclay's Toxicity to Their Physical and Chemical Properties. *ACS Appl. Mater. Interfaces* **2017**, *9*, 32323−32335.
(38) Pavan, C.; Fubini, B. Unveiling the Variability of "Quartz Hazard" in Light of Recent Toxicological Findings. *Chem. Res. Toxicol.* **2017**, *30*, 469−485.
(39) Verma, N. K.; Moore, E.; Blau, W.; Volkov, Y.; Babu, P. R. Cytotoxicity Evaluation of Nanoclays in Human Epithelial Cell Line A549 Using High Content Screening and Real-Time Impedance Analysis. *J. Nanopart. Res.* **2012**, *14*, 1137−1148.
(40) Dlugosz, M.; Kwiecien, A.; Zmudzki, P.; Bober, B.; Krzek, J.; Bialczyk, J.; Nowakowska, M.; Szczubiałka, K. A Hybrid Adsorbent/Visible Light Photocatalyst for the Abatement of Microcystin-LR in Water. *Chem. Commun. (Cambridge, U. K.)* **2015**, *51*, 7649−7652.
(41) Warheit, D. B.; Webb, T. R.; Colvin, V. L.; Reed, K. L.; Sayes, C. M. Pulmonary Bioassay Studies with Nanoscale and Fine-Quartz Particles in Rats: Toxicity Is Not Dependent upon Particle Size But Surface Characteristics. *Toxicol. Sci.* **2007**, *95*, 270−280.
(42) Schreider, J. P.; Culbertson, M. R.; Raabe, O. G. Comparative Pulmonary Fibrogenic Potential of Selected Particles. *Environ. Res.* **1985**, *38*, 256−274.
(43) Xie, W.; Gao, Z.; Pan, W. P.; Hunter, D.; Singh, A.; Vaia, R. Thermal Degradation Chemistry of Alkyl Quaternary Ammonium Montmorillonite. *Chem. Mater.* **2001**, *13*, 2979−2990.
(44) Raabe, O. G.; Al-Bayati, M. A.; Teague, S. V.; Rasolt, A. Regional Deposition of Inhaled Monodisperse Coarse and Fine Aerosol Particles in Small Laboratory Animals. *Ann. Occup. Hyg.* **1988**, *32*, 53−63.
(45) Winkler-Heil, R.; Hofmann, W. Modeling Particle Deposition in the Balb/c Mouse Respiratory Tract. *Inhalation Toxicol.* **2016**, *28*, 180−191.
(46) Mingelgrin, U.; Kliger, L.; Gal, M.; Saltzman, S. The Effect of Grinding on the Structure and Behavior of Bentonite. *Clays Clay Miner.* **1978**, *26*, 299−307.
(47) Evans, D. E.; Turkevich, L. A.; Roettgers, C. T.; Deye, G. J.; Baron, P. A. Dustiness of Fine and Nanoscale Powders. *Ann. Occup. Hyg.* **2013**, *57*, 261−277.
(48) Sanchez, V. C.; Jachak, A.; Hurt, R. H.; Kane, A. B. Biological Interactions of Graphene-Family Nanomaterials: An Interdisciplinary Review. *Chem. Res. Toxicol.* **2012**, *25*, 15−34.
(49) Schinwald, A.; Murphy, F. A.; Jones, A.; MacNee, W.; Donaldson, K. Graphene-Based Nanoplatelets: A New Risk to the Respiratory System as a Consequence of Their Unusual Aerodynamic Properties. *ACS Nano* **2012**, *6*, 736−746.

DOI: 10.1021/acsnano.7b07281
ACS Nano 2018, 12, 2292−2310

(50) Oscarson, D. W.; Van Scoyoc, G. E.; Ahlrichs, J. L. Effect of Poly-2-Vinylpyridine-N-Oxide and Sucrose on Silicate-Induced Hemolysis of Erythrocytes. *J. Pharm. Sci.* **1981**, *70*, 657−659.
(51) Porter, D. W.; Ramsey, D.; Hubbs, A. F.; Battelli, L.; Ma, J.; Barger, M.; Landsittel, D.; Robinson, V. A.; McLaurin, J.; Khan, A.; Jones, W.; Teass, A.; Castranova, V. Time Course of Pulmonary Response of Rats to Inhalation of Crystalline Silica: Histological Results and Biochemical Indices of Damage, Lipidosis, and Fibrosis. *J. Environ. Pathol., Toxicol. Oncol.* **2001**, *20*, 14.
(52) Castranova, V.; Porter, D.; Millecchia, L.; Ma, J. Y.; Hubbs, A. F.; Teass, A. Effect of Inhaled Crystalline Silica in A Rat Model: Time Course of Pulmonary Reactions. *Mol. Cell. Biochem.* **2002**, *234−235*, 177−184.
(53) Porter, D. W.; Hubbs, A. F.; Mercer, R.; Robinson, V. A.; Ramsey, D.; McLaurin, J.; Khan, A.; Battelli, L.; Brumbaugh, K.; Teass, A.; Castranova, V. Progression of Lung Inflammation and Damage in Rats After Cessation of Silica Inhalation. *Toxicol. Sci.* **2004**, *79*, 370−380.
(54) Willhite, C. C.; Karyakina, N. A.; Yokel, R. A.; Yenugadhati, N.; Wisniewski, T. M.; Arnold, A. M. F.; Momoli, F.; Krewski, D. Systematic Review of Potential Health Risks Posed by Pharmaceutical, Occupational and Consumer Exposures to Metallic and Nanoscale Aluminum, Aluminum Oxides, Aluminum Hydroxide and Its Soluble Salts. *Crit. Rev. Toxicol.* **2014**, *44*, 1−80.
(55) Kondej, D.; Sosnowski, T. R. Alteration of Biophysical Activity of Pulmonary Surfactant by Aluminosilicate Nanoparticles. *Inhalation Toxicol.* **2013**, *25*, 77−83.
(56) Mousseau, F.; Le Borgne, R.; Seyrek, E.; Berret, J. F. Biophysicochemical Interaction of a Clinical Pulmonary Surfactant with Nanoalumina. *Langmuir* **2015**, *31*, 7346−7354.
(57) De Saint Jean, M.; Brignole, F.; Bringuier, A. F.; Bauchet, A.; Feldmann, G.; Baudouin, C. Effects of Benzalkonium Chloride on Growth and Survival of Chang Conjunctival Cells. *Invest. Ophthalmol. Visual Sci.* **1999**, *40*, 619−630.
(58) Boston, M.; Dobratz, E. J.; Buescher, E. S.; Darrow, D. H. Effects of Nasal Saline Spray on Human Neutrophils. *Arch. Otolaryngol., Head Neck Surg.* **2003**, *129*, 660−664.
(59) Ho, C. Y.; Wu, M. C.; Lan, M. Y.; Tan, C. T.; Yang, A. H. *In Vitro* Effects of Preservatives in Nasal Sprays on Human Nasal Epithelial Cells. *Am. J. Rhinol.* **2008**, *22*, 125−129.
(60) Sharma, A. K.; Schmidt, B.; Frandsen, H.; Jacobsen, N. R.; Larsen, E. H.; Binderup, M. L. Genotoxicity of Unmodified and Organo-Modified Montmorillonite. *Mutat. Res., Genet. Toxicol. Environ. Mutagen.* **2010**, *700*, 18−25.
(61) Maisanaba, S.; Gutierrez-Praena, D.; Pichardo, S.; Moreno, F. J.; Jorda, M.; Cameán, A. M.; Aucejo, S.; Jos, A. Toxic Effects of a Modified Montmorillonite Clay on the Human Intestinal Cell Line Caco-2. *J. Appl. Toxicol.* **2014**, *34*, 714−725.
(62) Maisanaba, S.; Pichardo, S.; Jorda-Beneyto, M.; Aucejo, S.; Camean, A. M.; Jos, A. Cytotoxicity and Mutagenicity Studies on Migration Extracts from Nanocomposites with Potential Use in Food Packaging. *Food Chem. Toxicol.* **2014**, *66*, 366−372.
(63) Antonini, J. M.; Stone, S.; Roberts, J. R.; Chen, B.; Schwegler-Berry, D.; Afshari, A. A.; Frazer, D. G. Effect of Short-Term Stainless Steel Welding Fume Inhalation Exposure on Lung Inflammation, Injury, and Defense Responses in Rats. *Toxicol. Appl. Pharmacol.* **2007**, *223*, 234−245.
(64) Cho, W. S.; Duffin, R.; Howie, S. E.; Scotton, C. J.; Wallace, W. A.; Macnee, W.; Bradley, M.; Megson, I. L.; Donaldson, K. Progressive Severe Lung Injury by Zinc Oxide Nanoparticles; The Role of Zn^{2+} Dissolution Inside Lysosomes. *Part. Fibre Toxicol.* **2011**, *8*, 27.
(65) Roberts, J. R.; Antonini, J. M.; Porter, D. W.; Chapman, R. S.; Scabilloni, J. F.; Young, S. H.; Schwegler-Berry, D.; Castranova, V.; Mercer, R. R. Lung Toxicity and Biodistribution of Cd/Se-ZnS Quantum Dots with Different Surface Functional Groups after Pulmonary Exposure in Rats. *Part. Fibre Toxicol.* **2013**, *10*, 5.
(66) Brandenberger, C.; Rowley, N. L.; Jackson-Humbles, D. N.; Zhang, Q.; Bramble, L. A.; Lewandowski, R. P.; Wagner, J. G.; Chen, W.; Kaplan, B. L.; Kaminski, N. E.; Baker, G. L.; Worden, R. M.; Harkema, J. R. Engineered Silica Nanoparticles Act as Adjuvants to Enhance Allergic Airway Disease in Mice. *Part. Fibre Toxicol.* **2013**, *10*, 26.
(67) Mukhopadhyay, S.; Hoidal, J. R.; Mukherjee, T. K. Role of TNFa in Pulmonary Pathophysiology. *Respir. Res.* **2006**, *7*, 125.
(68) Keane, M. P.; Strieter, R. M. The Importance of Balanced Pro-Inflammatory and Anti-Inflammatory Mechanisms in Diffuse Lung Disease. *Respir Res.* **2002**, *3*, 5.
(69) Liu, H.; Fang, H.; Wang, W.; Cheng, Y.; Zhang, Y.; Liao, H.; Yao, H.; Chao, J. Macrophage-derived MCPIP1Mediates Silica-Induced Pulmonary Fibrosis *via* Autophagy. *Part. Fibre Toxicol.* **2016**, *13*, 55.
(70) Umbright, C.; Sellamuthu, R.; Roberts, J. R.; Young, S. H.; Richardson, D.; Schwegler-Berry, D.; McKinney, W.; Chen, B.; Gu, J. K.; Kashon, M.; Joseph, P. Pulmonary Toxicity and Global Gene Expression Changes in Response to Sub-Chronic Inhalation Exposure to Crystalline Silica in Rats. *J. Toxicol. Environ. Health, Part A* **2017**, *80*, 1349−1368.
(71) Rincon, M.; Irvin, C. G. Role of Il-6 in Asthma and Other Inflammatory Pulmonary Diseases. *Int. J. Biol. Sci.* **2012**, *8*, 1281−1290.
(72) Xia, L.; Gu, W.; Zhang, M.; Chang, Y. N.; Chen, K.; Bai, X.; Yu, L.; Li, J.; Li, S.; Xing, G. Endocytosed Nanoparticles Hold Endosomes and Stimulate Binucleated Cells Formation. *Part. Fibre Toxicol.* **2016**, *13*, 63.
(73) Sabo-Attwood, T.; Ramos-Nino, M. E.; Eugenia-Ariza, M.; Macpherson, M. B.; Butnor, K. J.; Vacek, P. C.; McGee, S. P.; Clark, J. C.; Steele, C.; Mossman, B. T. Osteopontin Modulates Inflammation, Mucin Production, and Gene Expression Signatures after Inhalation of Asbestos in a Murine Model of Fibrosis. *Am. J. Pathol.* **2011**, *178*, 1975−1985.
(74) Wang, L.; Liu, H.; Jiao, Y.; Wang, E.; Clark, S. H.; Postlethwaite, A. E.; Gu, W.; Chen, H. Differences Between Mice and Humans in Regulation and the Molecular Network of Collagen, Type III, alpha-1 at the Gene Expression Level: Obstacles that Translational Research Must Overcome. *Int. J. Mol. Sci.* **2015**, *16*, 15031−15056.
(75) Luzina, I. G.; Todd, N. W.; Sundararajan, S.; Atamas, S. P. The Cytokines of Pulmonary Fibrosis: Much Learned, Much More to Learn. *Cytokine+* **2015**, *74*, 88−100.
(76) Tonning, H. O. Pneumoconiosis from Fuller's Earth; Report of a Case with Autopsy Findings. *J. Ind. Hyg.* **1949**, *31*, 41.
(77) Elmore, A. R. Final Report on the Safety Assessment of Aluminum Silicate, Calcium Silicate, Magnesium Aluminum Silicate, Magnesium Silicate, Magnesium Trisilicate, Sodium Magnesium Silicate, Zirconium Silicate, Attapulgite, Bentonite, Fuller's Earth, Hectorite, Kaolin, Lithium Magnesium Silicate, Lithium Magnesium Sodium Silicate, Montmorillonite, Pyrophyllite, and Zeolite. *Int. J. Toxicol.* **2003**, *22*, 37−102.
(78) Snipes, M. B.; Boecker, B. B.; McClellan, R. O. Retention of Monodisperse or Polydisperse Aluminosilicate Particles Inhaled by Dogs, Rats, and Mice. *Toxicol. Appl. Pharmacol.* **1983**, *69*, 345−362.
(79) Nel, A. E.; Mädler, L.; Velegol, D.; Xia, T.; Hoek, E. M.; Somasundaran, P.; Klaessig, F.; Castranova, V.; Thompson, M. Understanding Biophysicochemical Interactions at the Nano-Bio Interface. *Nat. Mater.* **2009**, *8*, 543−557.
(80) Sharma, A. K.; Mortensen, A.; Schmidt, B.; Frandsen, H.; Hadrup, N.; Larsen, E. H.; Binderup, M. L. In-Vivo Study of Genotoxic and Inflammatory Effects of the Organo-Modified Montmorillonite Cloisite 30B. *Mutat. Res., Genet. Toxicol. Environ. Mutagen.* **2014**, *770*, 66−71.
(81) Iyer, R.; Hsia, C. C. W.; Nguyen, K. T. Nano-Therapeutics for the Lung: State-Of-The-Art and Future Perspectives. *Curr. Pharm. Des.* **2015**, *21*, 5233−5244.
(82) Larsen, S. T.; Verder, H.; Nielsen, G. D. Airway Effects of Inhaled Quaternary Ammonium Compounds in Mice. *Basic Clin. Pharmacol. Toxicol.* **2012**, *110*, 537−543.
(83) Swiercz, R.; Halatek, T.; Stetkiewicz, J.; Wasowicz, W.; Kur, B.; Grzelinska, Z.; Majcherek, W. Toxic Effect in the Lungs of Rats after

DOI: 10.1021/acsnano.7b07281
ACS Nano 2018, 12, 2292−2310

Inhalation Exposure to Benzalkonium Chloride. *Int. J. Occup. Med. Environ. Health* **2013**, *26*, 647−656.
(84) Workman, A. D.; Cohen, N. A. The Effect of Drugs and Other Compounds on the Ciliary Beat Frequency of Human Respiratory Epithelium. *Amer J. Rhinol Allergy* **2014**, *28*, 454−464.
(85) Todd, N. W.; Luzina, I. G.; Atamas, S. P. Molecular and Cellular Mechanisms of Pulmonary Fibrosis. *Fibrog. Tissue Repair* **2012**, *5*, 11.
(86) Noskovičová, N.; Petřek, M.; Eickelberg, O.; Heinzelmann, K. Platelet-Derived Growth Factor Signaling in The Lung. From Lung Development and Disease to Clinical Studies. *Am. J. Respir. Cell Mol. Biol.* **2015**, *52*, 263−284.
(87) Zissler, U. M.; Esser-von Bieren, J.; Jakwerth, C. A.; Chaker, A. M.; Schmidt-Weber, C. B. Current and Future Biomarkers in Allergic Asthma. *Allergy (Oxford, U. K.)* **2016**, *71*, 475−494.
(88) Djeska, I.; Ceausu, R. A.; Gaje, P. N.; Cimpean, A. M.; Mederle, O.; Nicodin, A.; Tudorache, V.; Raica, M. The Reticular Network Contributes to The Staging of Idiopathic Lung Fibrosis. *Arh Biol. Nauka* **2013**, *65*, 1599−1604.
(89) Cotran, R. S.; Kumar, V.; Collins, T. Tissue Repair: Cellular Growth, Fibrosis, and Wound Healing. In *Pathologic Basis of Disease*; WB Saunders: Philadephia, PA, 1999; pp 89−112.
(90) Fubini, B.; Bolis, V.; Cavenago, A.; Volante, M. Physicochemical Properties of Crystalline Silica Dusts and Their Possible Implication in Various Biological Responses. *Scand J. Work Environ. Health* **1995**, *21*, 9−14.
(91) Nidai Ozes, O.; Mayo, L. D.; Gustin, J. A.; Pfeffer, S. R.; Pfeffer, L. M.; Donner, D. B. NF-κB Activation by Tumour Necrosis Factor Requires The Akt Serine−Threonine Kinase. *Nature (London, U. K.)* **1999**, *401*, 82−85.
(92) Romashkova, J. A.; Makarov, S. S. NF-κB is a Target of AKT in Anti-Apoptotic PDGF Signaling. *Nature (London, U. K.)* **1999**, *401*, 86−90.
(93) Chung, K. F.; Adcock, I. M. Multifaceted Mechanisms in COPD: Inflammation, Immunity, and Tissue Repair and Destruction. *Eur. Respir. J.* **2008**, *31*, 1334−1356.
(94) Kyriakis, J. M.; Avruch, J. Mammalian MAPK Signal Transduction Pathways Activated by Stress and Inflammation: A 10-Year Update. *Physiol. Rev.* **2012**, *92*, 689−737.
(95) Shukla, A.; Timblin, C. R.; Hubbard, A. K.; Bravman, J.; Mossman, B. T. Silica-Induced Activation of c-Jun-NH_2-terminal Amino Kinases, Protracted Expression of the Activator Protein-1 Proto-Oncogene, fra-1, and S-Phase Alterations Are Mediated *via* Oxidative Stress. *Cancer Res.* **2001**, *61*, 1791−1795.
(96) Ding, M.; Shi, X.; Dong, Z.; Chen, F.; Lu, Y.; Castranova, V.; Val Vallyathan, V. Freshly Fractured Crystalline Silica Induces Activator Protein-1 Activation Through ERKs and p38 MAPK. *J. Biol. Chem.* **1999**, *274*, 30611−30616.
(97) Dong, X.; Liu, Y.; Du, M.; Wang, Q.; Yu, C. T.; Fan, X. P38 Mitogen-Activated Protein Kinase Inhibition Attenuates Pulmonary Inflammatory Response in a Rat Cardiopulmonary Bypass Model. *Eur. J. Cardiothorac Surg* **2006**, *30*, 77−84.
(98) Skuland, T.; Ovrevik, J.; Låg, M.; Schwarze, P.; Refsnes, M. Silica Nanoparticles Induce Cytokine Responses in Lung Epithelial Cells Through Activation of a p38/TACE/TGF-α/EGFR-Pathway and NF-κB Signaling. *Toxicol. Appl. Pharmacol.* **2014**, *279*, 76−86.
(99) Chen, F.; Shi, X. NF-kappaB, a Pivotal Transcription Factor in Silica-Induced Diseases. *Mol. Cell. Biochem.* **2002**, *234−235*, 169−176.
(100) Man, S. M.; Kanneganti, T. D. Converging Roles of Caspases in Inflammasome Activation, Cell Death and Innate Immunity. *Nat. Rev. Immunol.* **2016**, *16*, 7−21.
(101) Sayan, M.; Mossman, B. T. The NLRP3 Inflammasome in Pathogenic Particle and Fibre-Associated Lung Inflammation and Diseases. *Part. Fibre Toxicol.* **2015**, *13*, 51.
(102) Hanada, T.; Yoshimura, A. Regulation of Cytokine Signaling and Inflammation. *Cytokine Growth Factor Rev.* **2002**, *13*, 413−421.
(103) Kensler, T. W.; Wakabayashi, N.; Biswal, S. Cell Survival Responses to Environmental Stresses *via* the Keap1-Nrf2-ARE Pathway. *Annu. Rev. Pharmacol. Toxicol.* **2007**, *47*, 89−116.
(104) Bergsbaken, T.; Fink, S. L.; Cookson, B. T. Pyroptosis: Host Cell Death and Inflammation. *Nat. Rev. Microbiol.* **2009**, *7*, 99−109.
(105) Rastrick, J.; Birrell, M. The Role of the Inflammasome in Fibrotic Respiratory Diseases. *Minerva Med.* **2014**, *105*, 9−23.
(106) Brusselle, G. G.; Provoost, S.; Bracke, K. R.; Kuchmiy, A.; Lamkanfi, M. Inflammasomes in Respiratory Disease: From Bench To Bedside. *Chest* **2014**, *145*, 1121−1133.
(107) Saber, A. T.; Jacobsen, N. R.; Jackson, P.; Poulsen, S. S.; Kyjovska, Z. O.; Halappanavar, S.; Yauk, C. L.; Wallin, H.; Vogel, U. Particle-Induced Pulmonary Acute Phase Response May Be The Causal Link Between Particle Inhalation and Cardiovascular Disease. *Wiley Interdiscip Rev: Nanomed Nanobiotechnol* **2014**, *6*, 517−531.
(108) Poursafa, P.; Kelishadi, R. Air Pollution, Platelet Activation and Atherosclerosis. *Inflammation Allergy: Drug Targets* **2010**, *9*, 387−392.
(109) Tablin, F.; den Hartigh, L. J.; Aung, H. H.; Lame, M. W.; Kleeman, M. J.; Ham, W.; Norris, J. W.; Pombo, M.; Wilson, D. W. Seasonal Influences on CAPs Exposures: Differential Responses in Platelet Activation, Serum Cytokines and Xenobiotic Gene Expression. *Inhalation Toxicol.* **2012**, *24*, 506−517.
(110) Shah, A. D.; Denaxas, S.; Nicholas, O.; Hingorani, A. D.; Hemingway, H. Low Eosinophil and Low Lymphocyte Counts and the Incidence of 12 Cardiovascular Diseases: a CALIBER Cohort Study. *Open Heart* **2016**, *3*, e000477.
(111) Raynor, P. C.; Cebula, J. I.; Spangenberger, J. S.; Olson, B. A.; Dasch, J. M.; D'Arcy, J. B. Assessing Potential Nanoparticle Release During Nanocomposite Shredding Using Direct-Reading Instruments. *J. Occup. Environ. Hyg.* **2012**, *9*, 1−13.
(112) Cohen, J.; Deloid, G.; Pyrgiotakis, G.; Demokritou, P. Interactions of Engineered Nanomaterials in Physiological Media and Implications for *In Vitro* Dosimetry. *Nanotoxicology* **2013**, *7*, 417−431.
(113) Wang, L.; Castranova, V.; Mishra, A.; Chen, B.; Mercer, R. R.; Schwegler-Berry, D.; Rojanasakul, Y. Dispersion of Single-Walled Carbon Nanotubes by A Natural Lung Surfactant for Pulmonary *In Vitro* and *In Vivo* Toxicity Studies. *Part. Fibre Toxicol.* **2010**, *7*, 31.
(114) Soo, J. C.; Lee, T.; Chisholm, W. P.; Farcas, D.; Schwegler-Berry, D.; Harper, M. Treated and Untreated Rock Dust: Quartz Content and Physical Characterization. *J. Occup. Environ. Hyg.* **2016**, *13*, 201−207.
(115) Smulders, S.; Kaiser, J. P.; Zuin, S.; Van Landuyt, K. L.; Golanski, L.; Vanoirbeek, J.; Wick, P.; Hoet, P. H. Contamination of Nanoparticles by Endotoxin: Evaluation of Different Test Methods. *Part. Fibre Toxicol.* **2012**, *9*, 41.
(116) Zeidler-Erdely, P. C.; Antonini, J. M.; Meighan, T. G.; Young, S. H.; Eye, T. J.; Hammer, M. A.; Erdely, A. Comparison of Cell Counting Methods in Rodent Pulmonary Toxicity Studies: Automated and Manual Protocols and Considerations for Experimental Design. *Inhalation Toxicol.* **2016**, *28*, 410−420.

DOI: 10.1021/acsnano.7b07281
ACS Nano 2018, 12, 2292−2310